Modelling of brachytherapy needle deflection

Carolina Avila Carrasco

A dissertation submitted in partial fulfilment of the requirements of the University of the West of England, Bristol for the Degree of Master of Science in Robotics

Faculty of Engineering, University of the West of England, Bristol

September 2019

Declaration:

This study was completed for the MSc in Robotics by the University of the West of England, Bristol. The work is my own. Where the work of others is used or drawn on it is attributed.

The dissertation may be made freely available immediately for academic purposes.

Carolina Avila Carrasco

The number of words of this dissertation (main text) is 15,062.

Abstract

Brachytherapy is a localized radiotherapy procedure to treat cancer through the implantation of radioactive seeds in the affected tissue using dedicated needles. Accurate implantation of the seeds is critical for the treatment to be successful; however, needle deflection and soft tissue deformation during the insertion process produce deviations from the planned targets which might affect the effectiveness of treatment. The use of robotic brachytherapy systems with real-time tracking and control of needle trajectory is expected to improve the accuracy of this type of treatment. Online tracking of needle tip position would allow detection of targeting errors and in the case of steerable needles, path correction. One way to track needle insertion is using clinical image guidance; however, real-time clinical image processing and 3D reconstruction of the needle path is computationally expensive. This has led to research of alternative solutions for effective tracking of the needle without the use of images. Within this context, the use of models to predict real-time needle tip deflection from measured input data like the reaction forces produced at the base of the needle during the insertion into soft tissue has shown a good performance in previous research. So far, this modelling approach has only been applied to predict deflection of asymmetric bevel tip needles in one plane.

The main aim of this research project was to develop an analytical model for online 3D tracking of the needle tip position in symmetric brachytherapy needles. A model based on beam deflection theory has been developed which estimates needle tip deflection in two perpendicular axes, allowing for 3D tracking of the tip along the insertion process. The inputs to the model are the reaction shear forces and bending moments at the base of the needle, the insertion depth and some needle parameters (length, Young's Modulus and moment of inertia). The forces acting on the inserted portion of the needle were defined after a comparative analysis of various load profiles and selection of the combination of forces producing the lowest deflection estimation errors. The model was experimentally verified using data obtained from more than 100 needle insertion tests with different needles and tissue properties. The evaluation results show that the proposed model is only reliable for deflection prediction in the softest tissue. The model has a poor performance for hard tissue or two-layer tissue samples. Furthermore, the model works better for metal than for plastic needles.

The second goal of this research was to investigate the effect of a number of factors on the deflection behaviour of symmetric brachytherapy needles and compare the findings with the existing state of the art. This was done through needle insertion tests into gelatine phantom tissue with an experiment design including the following factors: needle type (titanium vs. plastic), tissue hardness (gelatine concentrations of 5%, 10% and 20%), insertion speed (10mm/s and 15mm/s) and addition or not of a skin layer to the tissue sample. A complete test setup was designed and built to carry out these experiments where the actual position of the needle tip along insertion was optically tracked in two perpendicular planes with two video cameras. Needle tip deflection at a certain insertion depth was measured in both planes through image processing of the video frames corresponding to that depth.

Analysis of the deflection behaviour was focused on the tip deflection at the final insertion depth (97mm). Results show quite small deflection values for both types of needles, which are consistent with previous published values for symmetric tip needles. Plastic needles experience a significantly larger mean absolute deflection (2.53 ± 1.06 mm) compared to titanium needles (1.28 ± 0.65mm); indicating that plastic needles are less reliable for clinical use. Magnitude of total deflection increases with tissue hardness, although this effect is not linearly proportional and seems to indicate a reduction of the influence with increasing hardness. Neither the addition of a skin layer nor the variation of insertion speed tested in this study produced a significant effect on the amount of needle deflection.

The findings of this study contribute to expand the existing knowledge about which factors have a significant influence on the deflection behaviour of symmetric needles and how they affect to the magnitude of this deflection. This research has also developed an analytical model for estimation of 3D needle deflection from reaction loads measured at the base. However, in contrast to the accurate performance reported by some previous studies on the application of beam-theory models to brachytherapy needles with bevel tip geometry, the reliability of this modelling approach is quite limited when applied to symmetric needles.

Table of Contents

1. Introduction

Brachytherapy is a localized radiotherapy to treat cancer through the implantation of radioactive seeds at specific points inside and around the tumour tissue using dedicated needles. This technique is currently used to treat prostate (Figure 1), cervical, breast and skin cancer.

Targeting accuracy is a critical factor for the clinical success of the treatment. Placing the seeds at the wrong points implies delivering a different radiation dose which might be less effective on the tumour tissue (Cormack, 2000). However, most current brachytherapy procedures are done manually and have a limited positioning accuracy of 3-6 mm (Lehmann, 2013; Popescu 2015). This is mainly due to needle deflection and soft tissue motion and deformation during the insertion process. The need for effective surgical solutions that improve the targeting accuracy and clinical effectiveness of this surgical procedure has led to the development of robotic systems capable of tracking and steering the needle during the insertion process.

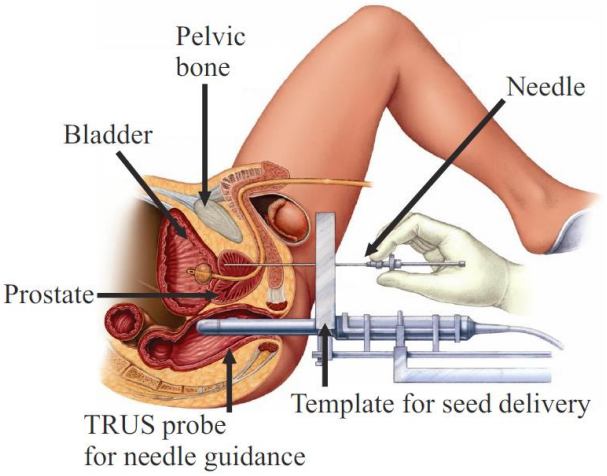

Figure 1. Brachytherapy procedure for prostate cancer treatment (Goksel, 2011).

Accurate control of needle insertion remains a challenge for brachytherapy robotic systems due to the needle bending, tissue deformation and the inherent variability of the process. Real-time needle tracking is necessary in order to detect deviations from the planned trajectory and, in the case of steerable needles, correct the trajectory accordingly to reach the final target. However, direct reliable needle tracking with physical sensors in a clinical setting without affecting the surgical process is not feasible with current technology.

Current brachytherapy procedures use image guidance for needle tracking, mainly ultrasound imaging although some systems also use MRI and CT guidance. This has boosted research on automated real-time image-guided tracking systems; however, image acquisition, processing and 3D reconstruction is a computationally expensive process. Real-time 3D tracking with sufficient accuracy is not feasible yet with current computer vision technology.

Therefore, research and development of alternative less computationally demanding solutions allowing online tracking of needle tip position would simplify the design of robotic needle insertion systems. In this context, the current research project aims to contribute to the development of future brachytherapy robotic tools capable of 3D tracking of needle tip during the insertion process without the need of computationally expensive image guidance technology.

The ultimate goal of this research project is to develop a model to predict deflection of symmetric brachytherapy needles along insertion into soft tissue from reaction loads measured at the base of the needle. Among all possible approaches, this work has focused on developing an analytical model based on beam deflection theory; establishing an equivalence between the needle and a cantilever beam. A similar approach has been previously applied by other researchers to predict the deflection of steerable beveled tip needles; however, there are no published studies about deflection models for symmetric tip needles. Symmetric tip needles are designed to minimize deflection under translational insertion in contrast to steerable beveled tip needles, which bend significantly more but whose deflection can be reduced by applying rotational motion around the needle axis during the insertion process. Despite the lower deflection and lack of steerability characterizing symmetric tip needles, quantification of the targeting error in this type of needle would still provide valuable information within a clinical context: It would help to identify those cases where targeting error is over an acceptable limit to deliver an accurate radiotherapy treatment; allowing the surgeon to correct seed implantation by repeating the insertion process.

Additionally, this study aims to characterize experimentally the deflection behaviour of brachytherapy symmetric tip needles; evaluating the level of influence that a number of factors have on the needle deflection. This knowledge will provide a better understanding about which aspects characterizing needle insertion procedures have a significant influence on targeting errors.

This dissertation starts with a review of the literature split into two blocks matching each of the research objectives of the project. The first block covers current research methods to measure or estimate needle deflection during insertion into soft tissue without the use of image guidance; with especial attention on models for needle deflection behaviour. The beam-theory modelling approach selected for this study is explained in more detail, together with a summary of previous studies using this type of model. The second literature block reviews the current knowledge on the factors that influence needle deflection with a summary of published results.

Chapter 3 describes the research methodology applied to fulfil the research objectives. The first part of the chapter explains the experimental setup to carry out needle insertion tests, the ground truth method used to measure needle deflection and the experiment design to evaluate the effect of different factors on needle deflection. The second part covers the definition of the deflection model and the methodology followed to evaluate the performance and reliability of this model with experimental data.

Results from the study are described in chapter 4, also divided according to the research objectives. Results from the needle insertion tests and statistical analysis of the effect of different factors on needle deflection are presented first. The second part explains the process for selection of the final deflection estimation model from a comparative performance analysis of different model variants; finally, results from a reliability evaluation of the proposed model are explained.

Chapter 5 contains a discussion of the results with separate analyses. First, results from the experimental characterization of needle deflection behaviour and influence of different factors are analysed and compared to previous literature. Second, the adequacy of the proposed deflection model for different needles and tissue properties is analysed in more detailed, followed by a discussion on the reliability of the proposed model and the beam-theory modelling approach in general. The last chapter summarises the work done with the main conclusions that can be derived from the results. Finally, a list of recommendations for future research on the topic is included.

2. Literature Review

Measurement of needle deflection without clinical imaging

Methods for real-time tracking of brachytherapy needles along the insertion process into soft tissue without using image guidance can be split into direct measurement methods and indirect measurement or estimation through the use of models.

Direct measurement methods rely on the use of **physical sensors embedded or attached to the needles**; mainly 'Electromagnetic (EM) tracking' sensor coils placed inside the needle (Abolhassani, 2007-(1); Sadjadi, 2014). This EM systems allow real-time 3D tracking; however, they are quite sensitive to the presence of metals, which can produce significant distortion and noise in the signal. Sadjadi (2014) proposed a method combining a needle deflection model with data collected from EM sensors using Kalman filters. They reported a 52% average tracking error reduction using this sensor fusion technique compared to model-based only estimations. However, the method was deemed not reliable for accurate estimation due to drift problems with the sensors. From a clinical use perspective, placing sensors inside brachytherapy needles doesn't seem the most adequate method, since this could hamper the load of radioactive seeds within the needle after insertion.

An alternative approach to direct measurement with sensors within the needle is to **predict needle deflection through needle-tissue interaction models and real-time input data** obtained through less invasive sensors. Modelling of needle insertion can be divided into three research areas: needle deflection, tissue deformation and needle-tissue interaction forces (Ravali, 2017). This study aims to develop a model for needle deflection behaviour, therefore literature review has focused on this area. Most of the existing modelling approaches for needle deflection are analytical and use mechanical principles. Webster (2006) proposed a nonholonomic kinematic model where the needle moves like a bicycle with a fixed curved trajectory (Figure 2). The curvature is defined by a constant front wheel angle and wheel base distance. These two parameters need to be fit with experimental data before using the model, which is a drawback for clinical application since it would require previous experimental characterization of each needle and tissue combination. This model is suitable for flexible bevel tip needles, which experience a significant deflection during insertion.

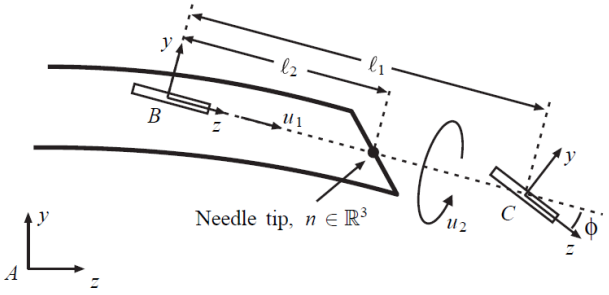

Figure 2. Bicycle-like nonholonomic model proposed by Webster (2006).

A different approach was proposed by Glozman (2007), who modelled the needle as a beam split into a series of linear beam elements supported by virtual linear springs simulating needle-tissue interaction forces (Figure 3). The stiffness coefficients characterizing the springs are obtained experimentally through image processing of the needle shape and calculation of the displacement of the virtual spring points from the reference straight line. This method is mainly thought for highly flexible needles where the shaft can change shape along the path. It requires clinical image to adjust model parameters from the needle shape, adding more complexity to the estimation of needle deflection.

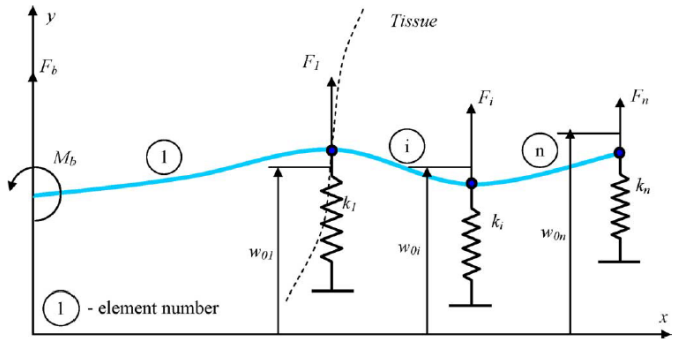

Figure 3. Model proposed by Glozman (2007): flexible beam supported by a number of virtual linear springs.

Goksel (2009) developed an 'angular springs' model where the needle is split into small rigid rods connected by spring-loaded joints. Consecutive needle segments bend and twist relative to each other by the action of external loads. Two rotational springs at each joint simulate the internal reaction torques or resistance of the needle shaft to bend or twist. The spring constants need to be obtained first through fitting of experimental data, which reduces the potential for clinical application of this approach.

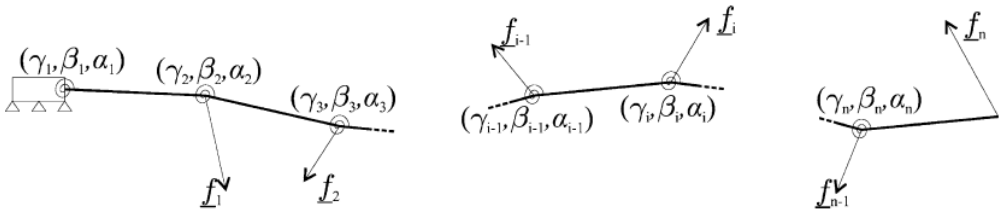

Figure 4. Angular springs model proposed by Goksel (2009).

Energy-based formulations have also been used to model needle deflection behaviour. Misra (2010) created a 2D model for flexible bevel tip needles where the total energy of the system (sum of energies due to needle bending and needle-tissue interaction forces minus the work done by the insertion forces and cutting forces at the tip) is expressed in terms of the transverse and axial deflections of the needle. Inputs of the model are the material and geometric properties of both, the needle and the tissue.

Finally, models based on Euler-Bernoulli beam theory have also been applied for estimation of needle deflection; establishing an equivalence between the needle and a cantilever beam. A summary of beam deflection theory foundations is explained in **Appendix 1**. The deflection of the needle can be related

to the loads acting on the needle along the insertion into soft tissue. In contrast to previously described models, which have mainly been applied to flexible needles that experience a significant deflection and curvature, application of beam-type models is only acceptable for rigid or almost-rigid needles where deflection is significantly low with regard to the total length of the needle (key assumption for the application of beam-theory equations). Needles used for brachytherapy procedures are rigid enough and experience sufficiently small deflections to meet beam-theory requirements. Among different analytical approaches, the **beam-theory modelling approach** has been selected for this research work since it is computationally less demanding than models that need medical images processing and does not require previous characterization of tissue mechanical properties. Only three parameters describing the needle (Length, Young's Modulus and Moment of inertia) and the measurement of bending reaction loads at the base are needed. This allows high sampling rates and real-time estimation of the needle tip position, hence offering potential for clinical application.

Previous research with beam-theory models:

Kataoka (2001) was the first proposing a needle deflection model based on beam-theory. They assumed that deflection is due to a tissue resistance force having a uniform load distribution along the inserted portion of the needle (Figure 5). This 2D model predicted needle deflection as a function of the measured transverse force at the base of the needle, the insertion length and needle diameter. However, deflection was underestimated by an offset of 2mm, indicating that the proposed force distribution profile was not representative enough of actual needle-tissue interaction forces. The authors suggested that a model using an alternative force distribution profile should improve deflection prediction.

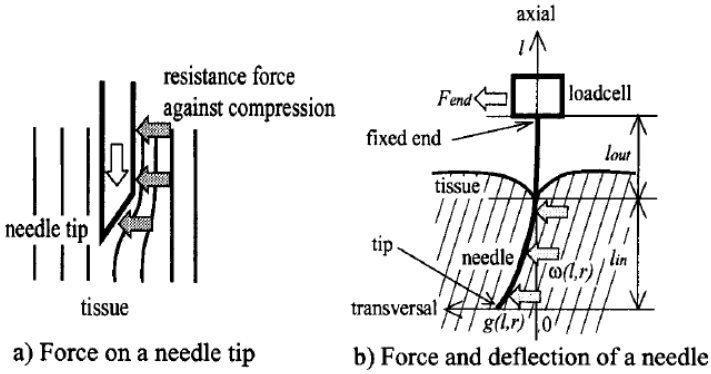

Figure 5. Needle-tissue interaction at deflection model proposed by Kataoka (2001).

Abolhassani (2007-(1)) also proposed a 2D deflection model for brachytherapy beveled-tip needles using beam theory equations and the reaction loads measured at the base. Although they initially considered a triangular vertical tissue resistance force distribution along the needle (included in the graphical representation of Figure 6), they finally assumed this load was negligible, with the cutting force at the tip being the main action responsible for needle bending.

They validated their model with needle insertion tests using a mechatronic system allowing translation and rotation of the needle; including a load-cell attached to the base of the needle to measure reaction

forces and torques. Actual position of the needle's tip was measured with an electromagnetic sensor; used as ground truth method for validation. Average model prediction errors along 60 mm insertion depth were below 1 mm for beef muscle and pig's heart.

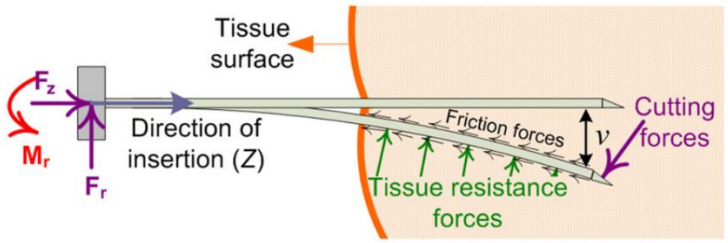

Figure 6. Representation of needle deflection model proposed by Abolhassani (2007-(1)).

The simplicity and low computational demands of beam-theory approach compared to real-time 3D image processing, led to further exploration by other research groups. Lehmann (2013, 2015, 2016-(1)) proposed and tested a number of model variants for deflection estimation of brachytherapy bevel tip needles in one plane. Different models used alternative force distribution profiles to represent needle-tissue interaction forces along the inserted length of the needle. Among all tested profiles, they obtained the best prediction accuracy for a combination of two load distributions: a uniform force and a triangular force (Figure 7-Right). Application of this model variant to needle insertion into gelatine phantom tissue and porcine loin muscle tissue resulted in estimation errors below 1mm for an insertion depth up to 130 mm for both types of tissue.

Review of existing literature on needle deflection models based on beam-theory shows that the most critical aspect is the definition of needle-tissue interaction forces. Some force profiles have shown better model performance than others although it seems that prediction errors could be reduced considering a dynamic load distribution profile that changed throughout the insertion process according to the load values instead of setting a fixed shape profile. However, identification of which load profile would be best for each insertion point in time is a challenge since direct measurement of needle-tissue interaction forces is not possible.

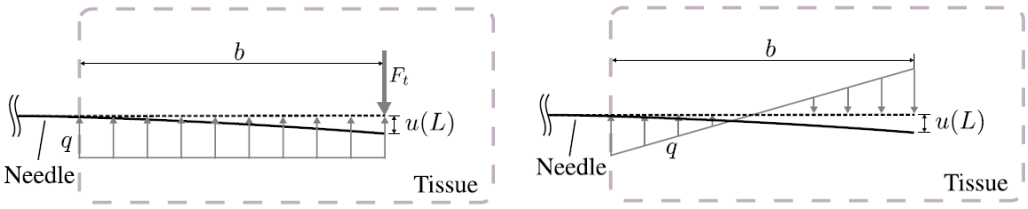

Figure 7. Two of the needle-tissue interaction profiles tested by Lehmann (2016-(1)). Left: Uniform force distribution and a cutting point force at the tip. Right: Combination of uniform and triangular force distributions.

There is a general agreement that needle-tissue interaction forces are distributed loads acting on the contact surface along the inserted portion of the needle; which can be split into normal and tangential forces (Figure 8). These forces result from tissue cutting by the needle tip surface, needle-tissue friction

and tissue resistance to compression. Published research about characterization of these interaction forces has mainly focused on the axial forces (Okamura, 2004; Podder, 2006; Abolhassani, 2007-(2); van Gerwen, 2012); probably because they are larger and simpler to model from external load measurements than the shear forces. Characterization and modelling of axial insertion forces has useful applications like providing haptic feedback to surgical simulators and robot-assisted surgery; however, it is the shear forces acting on the needle the ones responsible for needle bending and deviation from the planned trajectory. As mentioned above, accurate characterization of shear needle-tissue interaction forces along insertion hasn't been solved yet.

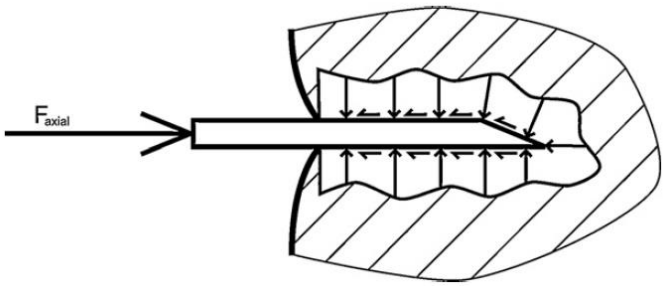

Figure 8. Graphical representation of the needle-tissue interaction forces during insertion (van Gerwen, 2012).

Factors that influence needle deflection

This study also aims to investigate the effect of certain parameters on the deflection behaviour of symmetric brachytherapy needles and compare the findings with existing published knowledge. Needle deflection is known to be affected by different factors that generally could be classified into: needle parameters, tissue properties and insertion parameters.

Needle parameters are those characterizing needle material and needle geometry, like the tip shape or needle diameter.

Tip geometry has shown high influence on needle deflection behaviour. Some of the typical needle tip geometries are shown in Figure 9, with the most popular designs for brachytherapy needles being the diamond, conical and bevel tips. Different authors have consistently found that bevel tip needles bend significantly more than symmetric tip needles (Okamura, 2004; Podder, 2005; van Veen, 2012). Typical deflection values observed for insertion depths of 100mm in artificial phantom tissues are close to 10 mm for bevel tip needles and close to 1 mm for symmetric needles (Podder, 2005; van Veen, 2012). The reason for larger deflection of bevel tip needles is their asymmetric geometry, which results in a transverse force from needle-tissue interaction at the tip causing the needle to bend when inserted into soft tissue. This predictable bending behaviour provides the steerability property to bevel tip needles, since their deflection can be controlled and reduced by applying rotational motion during insertion (Abolhassani, 2007-(3)). Among symmetric tip designs, diamond shape produces the lowest deflections

(≤1mm) and conical shape produces slightly larger deflections (≤3mm), with specific values depending on needle diameter, tissue properties and insertion conditions. The current study is focused on the behaviour of symmetric tip needles, specifically conical and diamond tip needles.

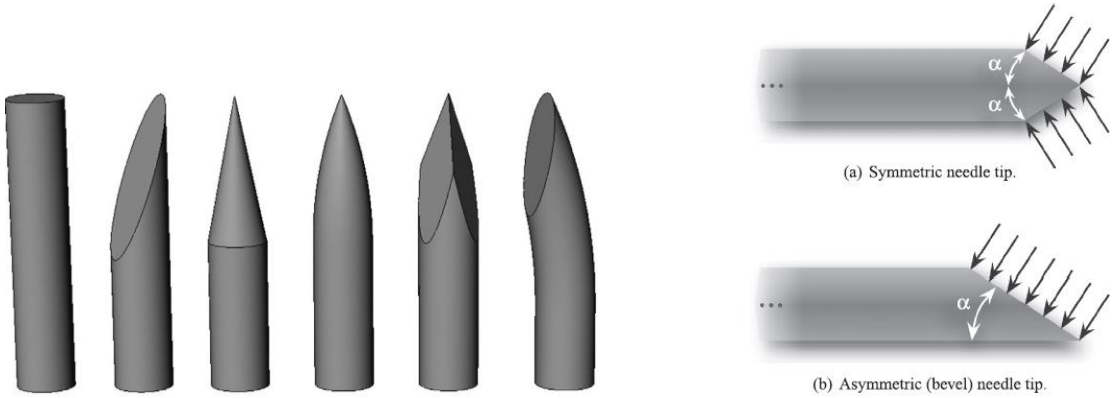

Figure 9. Left: Different types of tip geometries from left to right: blunt, beveled, conical, Sprotte, diamond, Tuohy (van Gerwen, 2012). Right: Different cutting force profiles for symmetric and asymmetric needle tips (Misra, 2010).

Published studies have found an inverse relationship between needle diameter and amount of deflection (Okamura, 2004; van Veen, 2012); the larger the needle diameter the less it bends. This is consistent with beam theory, since the amount of needle deflection is inversely proportional to the moment of inertia, therefore to the diameter.

With regard to the effect of needle material, no literature has been found that investigated this factor specifically. However, McGill (2012) studied the effect of the stiffness of the support rod onto which the hollowed needle is mounted. They measured higher tip deflections using a stainless steel core rod (Young's Modulus 200GPa) compared to using a much harder tungsten carbide rod (Young's Modulus 630GPa). This is also consistent with beam theory, since needle deflection is inversely proportional to the elastic modulus of the needle.

Among **tissue properties**, the influence of tissue hardness, heterogeneity and insertion through multiple tissue layers has been studied by different authors. There is a general agreement in the literature that tissue hardness has a significant effect on needle deflection, with harder tissues producing a larger amount of deflection (Podder, 2005; van Veen, 2012; Lehmann, 2015; Lehmann, 2016-(2)).

Experimental characterization of needle behaviour during insertion into soft tissue has been done with both, artificial and biological tissue. Artificial tissue phantoms can be made from different materials (silicone, PVC, agarose, gelatine, etc.) and usually have homogeneous physical properties. In contrast, animal and human biological tissues are characterized by their heterogeneity and it is expected this will produce a different behaviour of the needle in comparison to homogeneous tissue samples. De Jong (2015) studied the effect of tissue heterogeneity on needle deflection and found that both, mean and

variance of the absolute deflection were significantly higher for animal liver tissue than for homogeneous gelatine specimens.

Lee (2014) investigated the effect of insertion through multiple-layers by comparing insertions into homogeneous artificial tissue made of silicone gel, two-layer artificial tissue and porcine tissue with skin and muscle layers. They found larger needle deflection values in two-layer phantoms compared to homogeneous samples. They also found a significant influence of the thickness and stiffness of the upper layer: the thicker and harder the upper layer was, the larger the deviation of the final needle tip position from the planned target.

Lastly, **insertion parameters** include those elements associated to the insertion procedure, like insertion speed; the use of manual or robotic insertion; or the application of needle rotation simultaneously to linear insertion. Only the effect of insertion velocity has been included in the current review, since this is parameter of interest for the study and the experimental setup has been designed for a specific insertion method.

Literature is not conclusive regarding the effect of insertion velocity on needle deflection. Webster (2005) couldn't find a clear trend for insertion of flexible bevel tip needles when modifying speeds in a range of 5-25mm/s. Similarly Lemann (2013) found no influence of insertion speed on the amount of deflection for bevel tip brachytherapy needles between speed values of 10 and 15 mm/s. However, van Veen (2012) observed a 10% decrease of needle bending when increasing insertion speed from 5mm/s to 100mm/s and McGill (2012) also observed a reduction of needle deflection when increasing speed from 1120 mm/s to 2370 mm/s. According to published studies it could be hypothesized that insertion speed has a certain effect on needle deflection but it is only significant when comparing very different speed values.

3. Research Methodology

This project has two main research goals: A first objective is to investigate the influence of a number of factors on the deflection behaviour of symmetric tip needles when inserted into soft tissue. The second goal is to develop and evaluate an analytical model for 3D deflection prediction of symmetric tip needles.

This chapter explains the methodology followed to accomplish these research goals structured in two sections. The first section describes the materials and methods used for experimental characterization of needle deflection behaviour, including the experimental setup for needle insertion tests, the ground truth method to measure needle deflection, the experiment design to evaluate the effect of different factors of interest and the methods followed for data analysis. The second part covers the definition and experimental verification of the deflection model. Three model variants were defined and their prediction errors compared. The proposed final model is the best performance combination of those versions. The method followed to evaluate the performance and reliability of this final model is described.

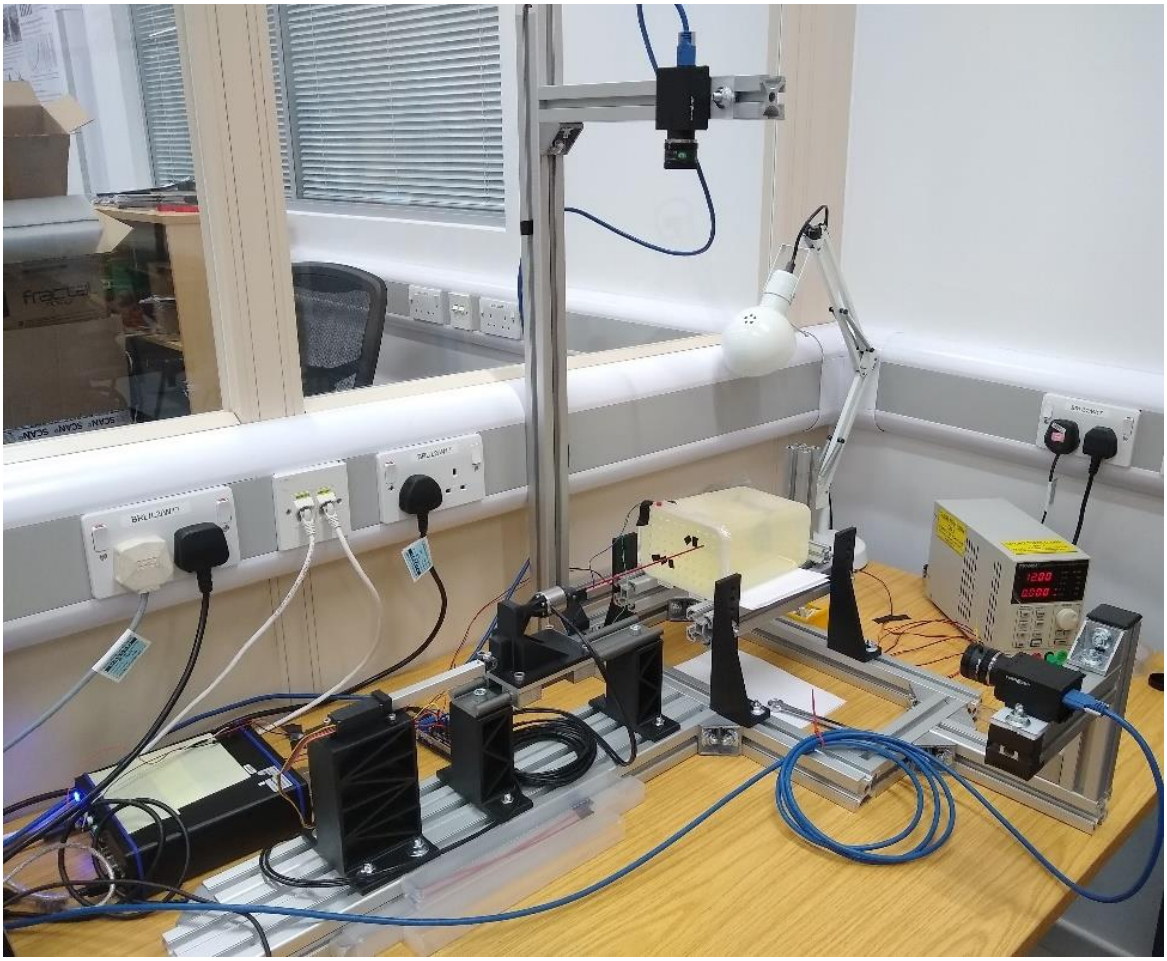

Figure 10. Experimental set-up for needle insertion tests designed and built for the study.

3.1. Experimental evaluation of needles deflection behaviour

3.1.1. Experimental set-up

A **mechatronic system** was designed and built to perform brachytherapy needles insertion into soft tissue samples up to a maximum depth of 100 mm approximately. A 6-axis load cell measures the reaction forces at the base of the needle along the insertion process, which is optically tracked by 2 video cameras (Figure 10).

The **mechanism for needle insertion** has one degree of freedom: translation along the needle axis, which is performed by a linear actuator with a potentiometer for position feedback (*Firgelli Model L16-100-63-12P*). It has a maximum stroke of 98 mm and a load capacity of 100 N, which are considered suitable for the intended application (maximum expected insertion loads are 20 N based on existing literature). The moving end of the linear actuator is attached to a sliding sub-assembly holding the needle and the load-cell at its base. A carriage-rail system (*IGUS drylin® double rail*) allows the displacement of the needle for insertion and retraction ensuring precise alignment (Figure 11).

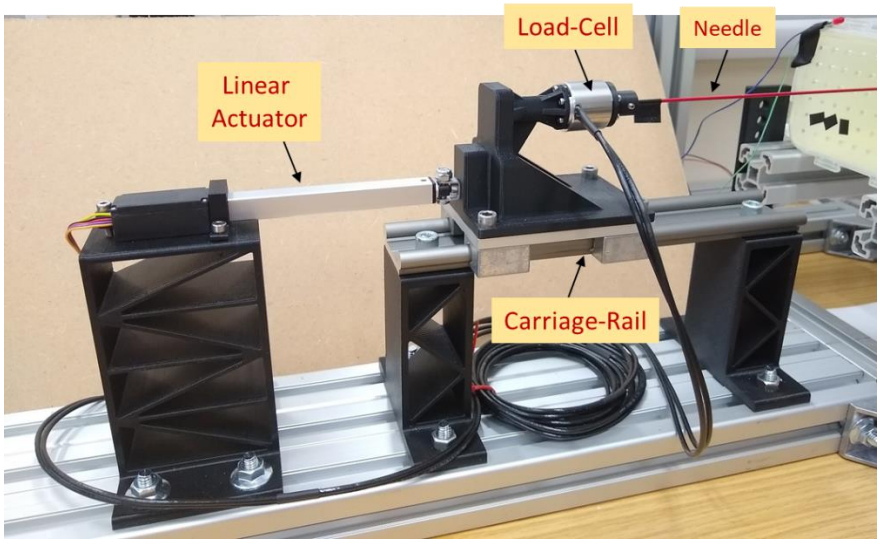

Figure 11. Detail of mechanism for needle insertion.

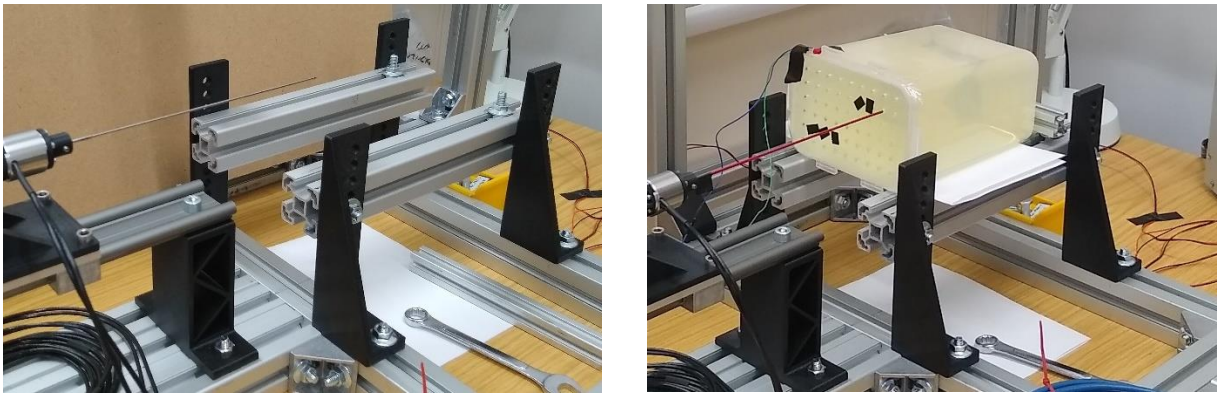

Figure 12. Adjustable support structure for tissue samples.

A metal structure made of aluminium profiles is used as common mounting frame for the needle insertion mechanism, the support platform for tissue samples and the video cameras (Figure 10). Phantom tissue samples are placed over an adjustable support structure which allows moving the sample up/down and left/right with regard to the needle axis, changing the location of the insertion point for every test (Figure 12).

The mechanism for needle insertion/retraction is controlled by an *Arduino Uno Rev.3* board combined with an *Arduino Motor Shield* to control the speed and direction of the linear actuator DC motor. Insertion depth is monitored through feedback position signal from the linear actuator potentiometer and insertion speed is set through pulse width modulation (PWM) of the motor speed analogue output signal. Insertion tests were carried out at two different speeds by setting two different PWM values which corresponded to 10 mm/s and 15mm/s average linear speed values.

A **6-axis load cell** (*Interface Model-6A27)* is fixed to the base of the needle holder and used for real-time measurement of reaction forces during the insertion tests (Figure 13). The cell has a load capacity of 200N for traction/compression forces, 50N for shear forces and 1Nm for all torques. The sensor is connected to a dedicated **data acquisition device** (DAQ) including signal conditioning and amplifier and allowing for synchronized sampling of all analogue inputs with 24 bit resolution (*Interface Model - BX8-HD44 BlueDAQ series*). It has USB connection to the PC, where load-cell measurements can be controlled, monitored and saved through the specific '*BlueDAQ'* data logging software. Acquisition frequency was set to 100 Hz for all insertion tests.

Figure 13. Left: Detail of Interface Load Cell fixed to the base of the needle; Right: Connection to PC through Data Acquisition System.

In addition to the load-cell measurements, the position signal of the linear actuator was also input to the DAQ through a shared connection with the *Arduino Uno* board. This way, a **synchronised reading between forces and needle insertion depth** is obtained for further data processing and analysis. The start and end of each needle insertion test are controlled by the *Arduino* board, which at the same time triggers and stops load-cell and insertion depth data acquisition by *BlueDAQ* device.

Figure 14 shows load-cell axes layout used in the experimental setup. X-axis is vertical with positive direction pointing downwards and perpendicular to the needle axis; Y-axis is horizontal and

perpendicular to the needle axis; Z-axis is coincident with the needle axis with positive direction pointing in the insertion direction. Measurements were referenced to the base of the needle by applying a geometric offset correction to the sensor's default reference frame. From the 6 load measurements, only forces and torque producing needle bending were used as inputs to the model for estimation of needle deflection: Shear force acting along X axis and torque in Y axis cause the needle bending in the vertical XZ plane; shear force along Y axis and torque in X axis produce needle bending in the horizontal YZ plane. Reaction forces and torques acting on the needle have opposite sign to those measured by the load-cell. These were also smoothed with a Savitzky-Golay low-pass filter.

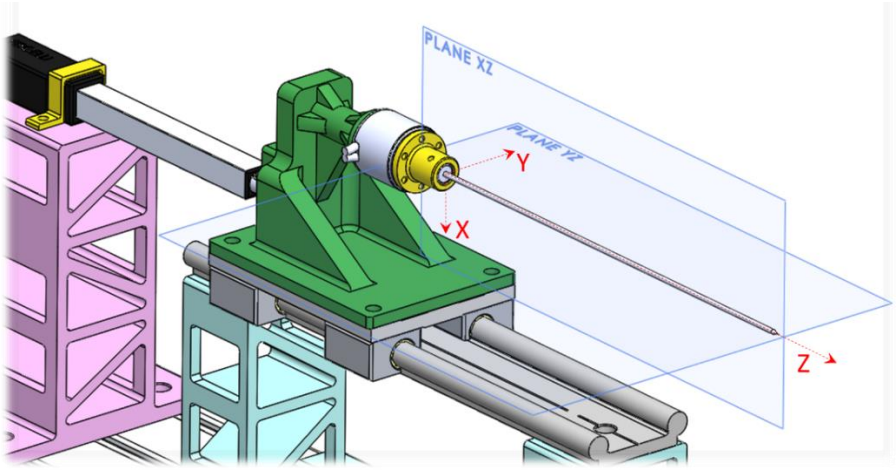

Figure 14. Load-cell Coordinate System axes layout. Origin set at needle's base.

Ground truth measurement of needle deflection:

Actual needle deflections along insertion tests were measured using optical tracking with video cameras. This method has been previously used in research studies to measure needle deflection when tissue samples are transparent (Webster, 2005; van Veen, 2012; Lehmann, 2013 & 2015). Some researchers have alternatively used EM sensors placed inside the needle tip (Abolhassani, 2007-(1); Sadjadi, 2014) but these are quite sensitive to the presence of metals, which can produce significant distortion in the signal. For that reason, optical tracking method was preferred for this study.

For each test, needle insertion was optically tracked with two video cameras (*PointGrey – Model: Grasshopper3 GS3-U3-41CEC*). Both cameras are fixed to the setup metal frame and placed orthogonal to each other in order to measure needle deflection in two perpendicular planes (Figure 15). These planes are coincident with the load-cell coordinate system XZ and YZ planes, allowing for direct comparison between needle deflections estimated by the model and ground truth measurements.

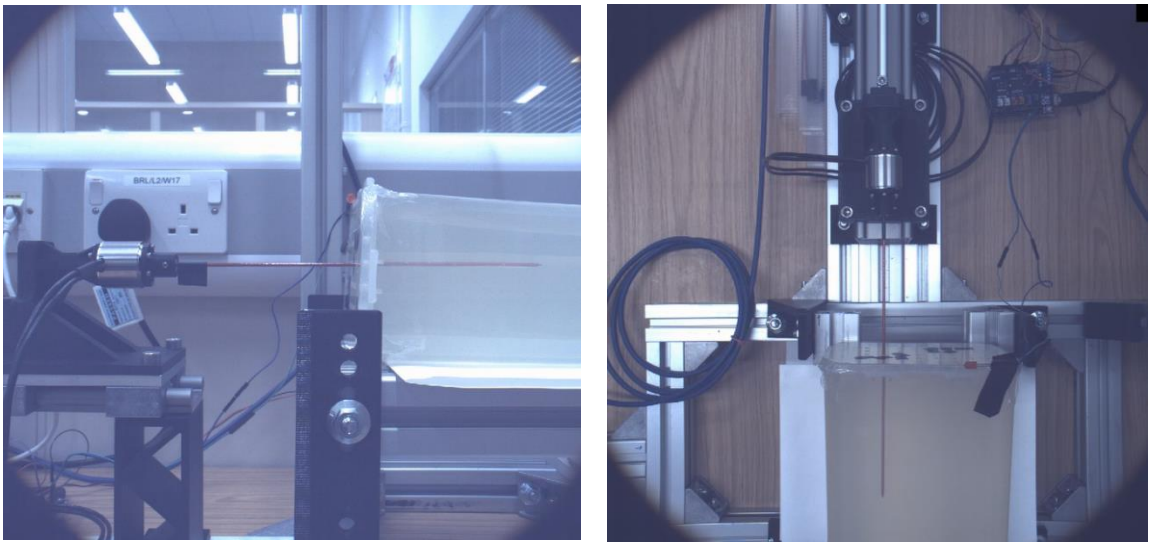

Figure 15. Field of view captured by each camera during insertion tests. Left: Camera for XZ vertical plane. Right: Camera for YZ horizontal plane.

Video capture was controlled through *Matlab Image Acquisition toolbox* and a specific script developed for the experiments which allows synchronization of both cameras. The acquisition frequency was set to 20 frames per second. Video acquisition was not synchronized with load-cell and insertion depth data but they were paired later through post-processing of video and data files. An LED flash light is triggered immediately before the linear actuator starts moving. This is captured by both cameras and is later used in the video processing to identify the timestamp marking the start of the insertion (insertion depth equal to zero). Identification of video frames corresponding to specific insertion depth values is achieved by the use of timestamps in both, video files and data acquisition files; allowing for adequate pairing of video, forces and insertion depth data.

Measurement of needle deflections:

Needle deflection has been defined as the Euclidean distance of needle tip from the needle axis in a perpendicular plane to needle axis (Figure 16). Total deflection can be split into planar components δx and δy, which quantify needle tip deflections along X-axis (vertical) and Y-axis (horizontal) respectively. The vector sum of these two components is the resultant needle deflection δt.

Needle deflection could be measured at any point along its length, characterizing the resulting curvature. Other authors have characterized needle deflection by measuring the curvature radius, but this is out of the scope of this research. Needle deflection will be characterized by the deviation of the tip from the needle trajectory, which quantifies needle targeting error.

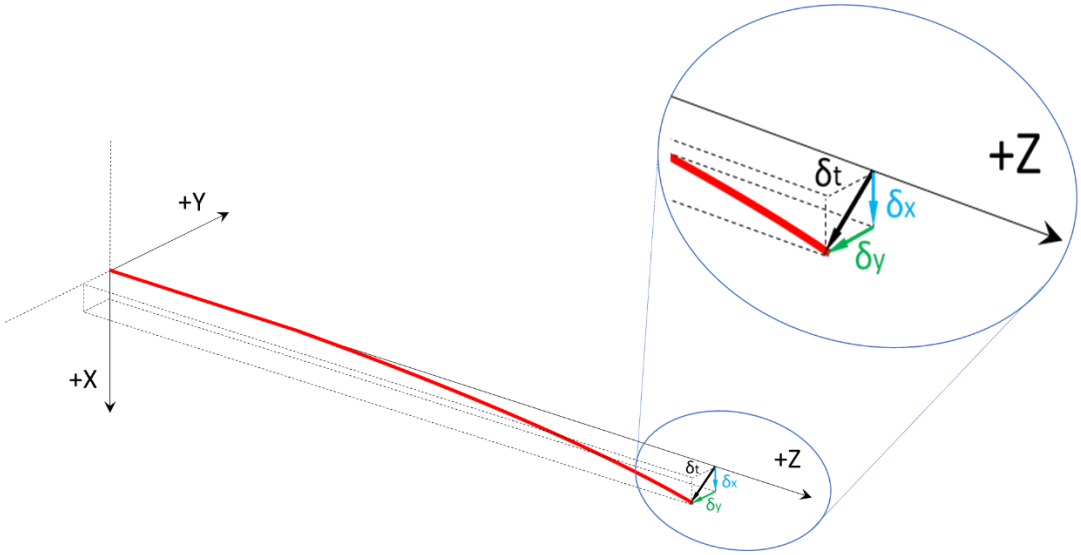

Figure 16. Graphical representation of needle deflection defined as the Euclidean distance of the needle tip from needle axis. Total needle deflection δt is the sum of perpendicular deflections δx and δy. Axes layout is the one adopted in this study.

Needle tip deflections in each plane of interest were measured using *Image Processing Tools* in *Matlab*. For each insertion depth value selected for analysis, the corresponding frames are extracted from the original video-files. A semi-automatic programme was written to measure needle deflection in each plane from two input points: needle axis base and needle tip. These two points are manually marked on an image display window and the programme calculates the deflection values defined as the perpendicular distance between the needle tip and needle axis on each plane (Figure 17). Previously to deflection measurements, image calibration was performed for each camera to find the ratio between the number of pixels and distance in mm.

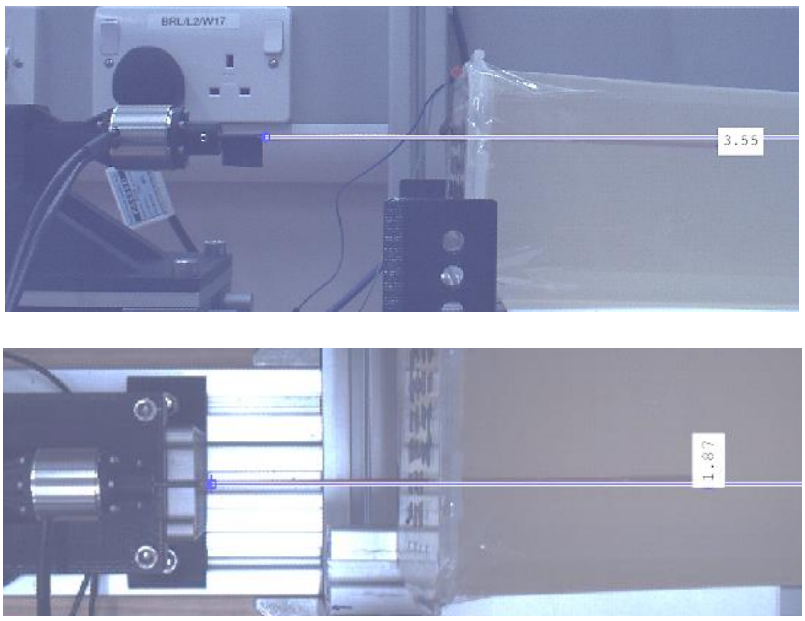

Figure 17. Example of results from image processing of needle insertion video-frames to extract the value of needle tip deflection in each plane.

Tip deflection was measured at four specific insertion depths: 25mm, 50mm, 75mm and final insertion depth of 97mm approximately. Actual deflection values were calculated as the difference between the needle tip deviation measured on the specific insertion depth frame and the initial tip deviation measured for insertion depth zero. That is, measured needle deflections are relative to the initial tip deflection at the start of the insertion.

Image resolution was set to 1024x1024 pixels in both cameras. This resulted in a measuring resolution of approximately 0.33mm for XZ plane and 0.40mm for YZ plane (with small variations depending on individual calibration conditions of each test). Repeatability of the method was assessed by repeating needle deflection measurements for a group of 20 tests. Average absolute differences between repeated measurements were 0.21 mm for images of plane XZ and 0.25mm for images of plane YZ. These are lower than the resolution values; however, maximum differences reached 0.5mm (XZ) and 0.65mm (YZ). This should be taken into account when comparing measured and model predicted deflection values, since prediction errors lower than 0.5 mm could be due to measurement errors.

Needles:

Two types of symmetric tip needles were used in the experimental study. Both needles are hollowed and need to be mounted onto a stainless steel core rod called 'mandrin', which holds the needle and provides support during the insertion process. In a real clinical scenario, once the needle is fully inserted, the mandrin is retracted and removed to allow for implantation of the radioactive seed within the tip of the needle. In this experimental setup, the base of the needle mandrin is fixed into a needle holder which is attached to the load cell.

1. **Plastic Needles of 200 mm length and 2 mm diameter** (*Varian Medical Systems*). They are made of PEEK and have conical tip geometry. Since their colour is very similar to that of gelatine tissue samples, tested needles were painted in red to improve their visibility for optical tracking. Three plastic needle samples were used in the insertion tests.

   It is worth mentioning that all plastic needles had a certain curvature as can be noticed in Figure 18. Although this curvature was significantly reduced when mounted onto the metal core, part of the curvature still remained, resulting in an appreciable deviation of the tip from the needle axis. As will be shown in the results section, this curvature defect had an effect on the final deflection of the plastic needles.

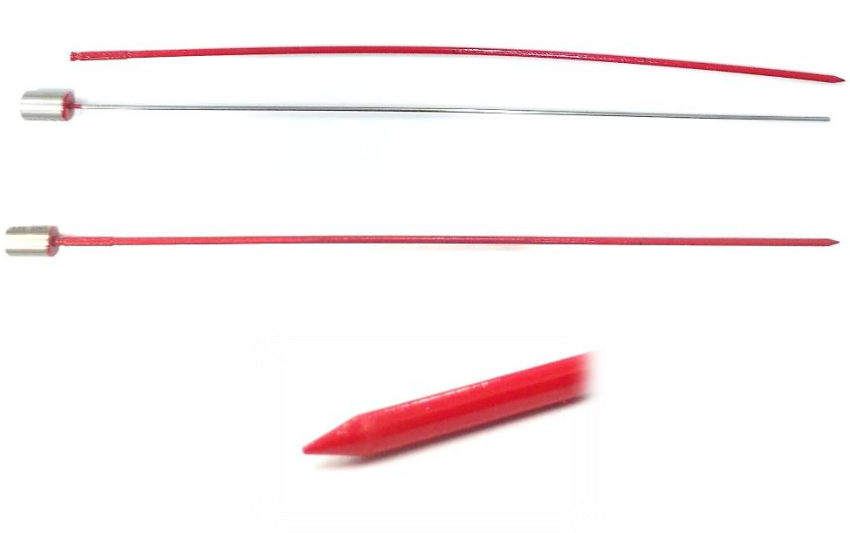

Figure 18. Plastic needle used in the study. Top: Needle + Mandrin core; Centre: Needle onto mandrin; Bottom: Detail of the conical tip geometry.

2. **Titanium Needle of 200 mm length and 16 Gauge** (1.65 mm) **diameter** (*Varian Medical Systems*). They have a sharp trocar or diamond shape tip. One Titanium needle was used for all the insertions.

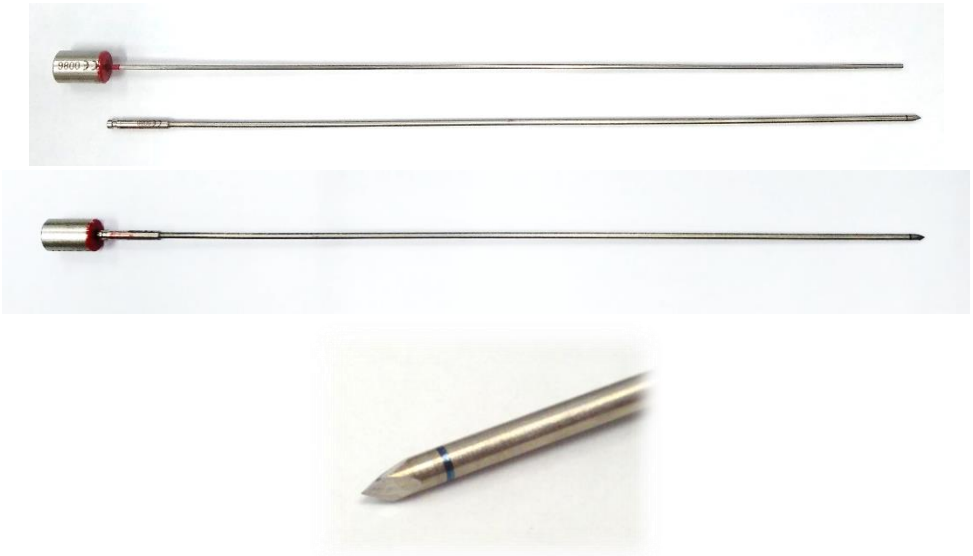

Figure 19. Titanium needle used in the study. Top: Needle + Mandrin core; Centre: Needle onto mandrin; Bottom: Detail of the trocar tip geometry.

Phantom tissue samples:

Phantom tissue samples were made of porcine gelatine (*ClassiKool 240 Bloom Pig Skin gelatine*). Three different hardness grades were obtained by mixing gelatine and water in different concentrations: 5%, 10% and 20%. Previous needle insertion studies have also used gelatine to simulate soft tissue, since it is considered representative enough of the body soft tissue properties (Podder, 2005; Misra, 2010; Lehmann, 2016-(1)).

Another aspect included in the experimental study is the analysis of the influence of two-layer insertion. An additional tissue layer simulating the skin was added on top of the soft-tissue phantom in some of the experiments in order to evaluate the effects on needle deflection. This 'skin layer' is approximately 5mm thick and is made of a silicone-like material representative of skin tissue hardness (*Superflab Plastic Bolus Material)*.

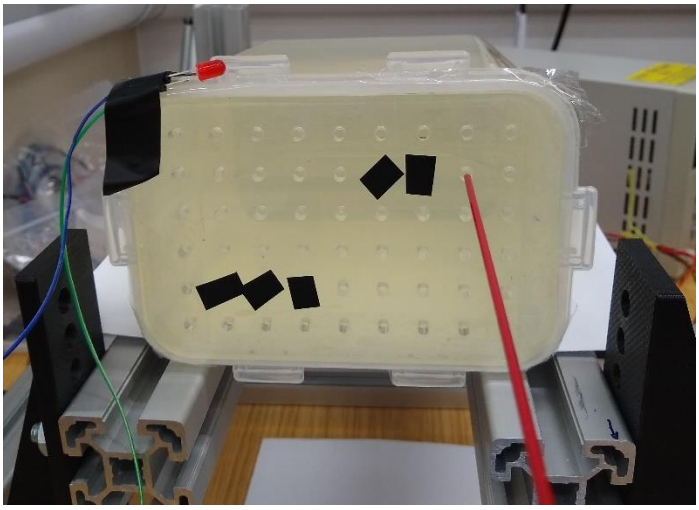

Figure 20. Phantom tissue sample with grid template on the front face.

Phantom tissue samples were built and tested inside a transparent plastic container. A hollowed plastic plate simulating a brachytherapy guiding grid template was fixed on top of the insertion face and used in all of the tests (Figure 20). This template consists of a grid of holes separated 12.5 mm from each other. This ensures that insertions into the same tissue sample are regularly spaced and the needle is always inserted into a different tissue region.

3.1.2. Experiments design

Needle insertion tests under different conditions were performed with a double purpose: evaluation of the needle deflection behaviour and verification of the proposed needle deflection model. As a first objective, the influence of the following factors on the amount of needle deflection was investigated:

1. **Needle type**: two different needles described in section 3.1.1 were tested. This factor combines the effects of needle material, tip geometry and diameter. The initial hypothesis for the study is that plastic needles should bend more than titanium needles despite having a larger diameter since they are more flexible (Young's Modulus almost four times lower) and the difference in the elastic modulus should have a stronger effect.

2. **Tissue hardness**: three different tissue densities were tested using gelatine concentrations of 5%, 10% and 20% as described before. Tissue hardness is directly proportional to gelatine concentration of the sample. It is initially hypothesized that absolute needle deflections will be larger for harder tissue samples according to previous published research.

3. **Skin layer**: insertion tests were carried out on samples with and without a skin layer in order to evaluate the effect of two-layer insertion. According to the existing literature, the initial hypothesis is that the addition of a skin layer will increase the amount of the needle deflection and variability of behaviour.

4. **Insertion speed**: for each needle type and tissue sample, two different insertion speeds were tested. For samples without skin layer, average speed values were 10 mm/s and 15mm/s. The addition of the skin layer produced a reduction of the insertion speeds of 2-3 mm/s due to the higher motor force required for insertion. To favour clarity in the analysis of the influence of this factor, insertion speed was considered as a categorical variable instead of numerical; distinguishing between 'Low' and 'High' speed values for each needle type and tissue sample. The initial hypothesis for this study is that needle deflection won't be significantly different between both insertion speeds.

The design of experiments considered combinations of these factors as per the experiments matrix shown in Table 1. More than 100 needle insertion tests were performed in the study. Combinations with skin layer were only tested for tissue densities 10% and 20%.

Needle	Tissue Density	Skin	Speed	Number of repetitions
Plastic	5%	No skin	Low	5
			High	5
	10%	With skin	Low	7
			High	7
		No skin	Low	5
			High	5
	20%	With skin	Low	5
			High	5
		No skin	Low	5
			High	5
Titanium	5%	No skin	Low	5
			High	5
	10%	With skin	Low	5
			High	5
		No skin	Low	5
			High	5
	20%	With skin	Low	5
			High	5
		No skin	Low	5
			High	5

Table 1. Experiments design: Different tested combinations of factors under analysis.

The analysis of the effect of the different factors was done for the **final needle tip deflection at the maximum insertion depth** (97 mm approximately). This is the maximum expected deflection value for each insertion test, hence the value with the highest discriminant potential when analysing possible differences among test conditions. Deflections at shorter insertion depths are expected to be very small and they might not show different needle behaviours as clearly. Final tip deflection was defined by three

variables: deflection along X-axis (δx), deflection along Y-axis (δy) and absolute total deflection calculated from the first two variables ($\delta t=\sqrt{(\delta x^2+ \delta y^2)}$). Deflections along X and Y axes were measured using the image processing method described in section 3.1.1.

Influence of the four factors under analysis on final needle deflection was evaluated through a descriptive statistical analysis of the mean and standard deviation (STD) of selected deflection variables for each group; followed by multi-way *Analysis of Variance* (ANOVA) tests and non-parametric *Kruskal-Wallis* tests. Statistical analysis was done with *Matlab 2017b* (*Statistics and Machine Learning Toolbox*) and "*R-Commander*" (*R-3.6.1*) software. More details about the statistical analysis of measured deflection data are included in the results section.

3.2. Deflection model

As explained in the literature review, the beam-theory approach was selected for the analytical deflection estimation model developed in this study. In order to find a suitable load profile for adequate modelling of needle-tissue interaction forces, three different model variants characterized by different load profiles acting on the inserted portion of the needle were considered for analysis.

3.2.1. Proposed model variants

Theory background:

The basic differential equation of the deflection curve of a beam which relates bending moment and deflection can be written as:

$$M = EI\frac{d^2v}{dx^2} \qquad \text{(Eq. 1)}$$

The deflection *v(x)* at any section of the beam at distance *x* from the base can be obtained by integrating twice this differential equation. The expression for the bending moment along the beam can be obtained from free-body diagrams and equilibrium equations. Depending on the nature of the loads acting on the beam, there might be one bending moment expression applicable to the entire beam or several moment expressions for different regions of the beam. In the latter case, a different equation for the deflection will result for each region of the beam.

A useful technique when calculating the deflection of a beam is to apply the principle of superposition. This states that "*under suitable conditions, the deflection of a beam produced by several different loads acting simultaneously can be found by superposing the deflections produced by the same loads acting separately*" (Gere, 2009). This simplifies the calculation process since deflections due to individual loads can be obtained more easily and in many cases, the formulas for deflections for typical load distributions are readily available in engineering books. Application of the principle of superposition is correct under the following assumptions: 1) the material is linearly elastic; 2) deflections and rotations

are small (*dv/dx<<1)*; 3) deflection does not alter the actions of the applied loads. These conditions ensure that the differential equations of the deflection curve are linear and the different loading conditions can be added algebraically (superposition is possible).

Application to needles deflection:

Application of beam deflection theory to model deflection behaviour of brachytherapy needles is considered acceptable since their mechanical behaviour is assumed to meet the above requirements for application of simplified beam-theory equations. Particularly in the case of symmetric needles, where expected deflections are notably small compared to the needle length.

Using beam-theory equations, three variants of a needle deflection model have been defined and compared with regard to their performance for the symmetric tip needles used in this study. The difference between these model variants lies in how needle-tissue interaction forces profile is defined. **The model estimates needle tip deflection (δ) in two perpendicular axes**: vertical deflection along X axis (δx) and horizontal deflection along Y axis (δy). Resultant 3D total deflection can be calculated as the vector sum of these deflections (Figure 16). Input data for the model are the reaction shear forces and bending moments at the base of the needle (derived from load-cell measurements), insertion depth (extracted from linear actuator potentiometer signal) and needle-dependent parameters like the length, Young's Modulus and area moment of inertia.

A common **methodology to calculate the needle tip deflection on each plane** was used for the three model variants:

1. First, needle tip deflection equation is defined based on the applied load profile and using the superposition principle when more than one type of load is acting on the needle. For some of the load profiles, deflection formulas were available from engineering books (Gere, 2009). When the formula was not available, the expression for needle deflection was obtained by double integration of the bending-moment equation (Eq. 1).
2. Second, the unknown forces acting on the needle are calculated from static equilibrium equations of all forces and moments acting on the needle.
3. The value of needle tip deflection is obtained by substituting the calculated forces and the rest of known parameters in the deflection equations.

The **sign conventions** adopted for shear forces, bending moments and deflections are as follows:

- Deflection is positive when happens in the positive direction of the corresponding coordinate frame axis and negative when happens in the negative direction of the axis.
- Forces in the positive direction of the corresponding axis are positive and vice versa.
- Bending moments are positive if produce a positive deflection and negative when produce a negative deflection.

Needle constant parameters used as inputs for the deflection models are the Young's Modulus *E*, the area moment of inertia *I* and the total length of the needle *L*.

Young's Moduli of both tested needles were obtained experimentally since they are not solid but hollowed and can be considered as made of composite materials due to the stainless steel core (mandrin). **Appendix 2** describes the methodology and data used to calculate the values of Young's Moduli. The average resulting values are 27,646 MPa for plastic needles and 107,735 MPa for titanium needles.

The area moment of inertia for each needle *I* was calculated as the sum of the moments of inertia of the mandrin core I_m and the hollowed needle I_n:

$$I_m = \pi . \emptyset_m{}^4/64 \qquad I_n = \pi . (\emptyset_{out}{}^4 - \emptyset_{in}{}^4)/64 \qquad I = I_m + I_n$$

These resulted in 0.7673 mm^4 for plastic needles and 0.3285 mm^4 for titanium needles.

Model 1: Uniform load distribution

This variant is characterized by a uniform load distribution along the inserted portion of the needle. This would result from unbalanced tissue compression forces around the needle. Under ideal conditions and insertion into homogeneous tissue, it is hypothesized that a symmetric needle would be subject to equal compression forces from surrounding tissue all around its section. This would result in a straight trajectory with no deflection. When there is an unbalance of these forces, a resultant force will appear and cause needle deflection. Figure 21 shows an example where the forces acting on the inserted portion of the needle in the plane of bending are not equal, producing a deflection as a consequence of the resultant uniform load distribution.

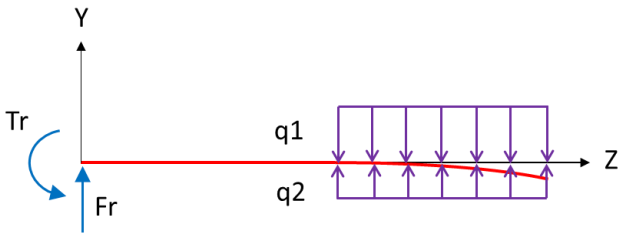

Figure 21. Unbalanced load distribution around the inserted portion of the needle would result in needle deflection. Needle profile in red.

Model 1 considers this resultant uniform load distribution along the inserted portion of the needle. Figure 22 shows a graphical representation of this model in both planes considered for deflection estimation. *L* represents the total length of the needle, *dp* is the inserted length and *a* is the length outside the tissue. Reaction loads at needle's base are force *Frx* and torque *Try* in the vertical plane XZ and force *Fry* and torque *Trx* in the horizontal plane YZ. The uniform load distribution has a force intensity per unit length of *qx* in plane XY and *qy* in plane YZ.

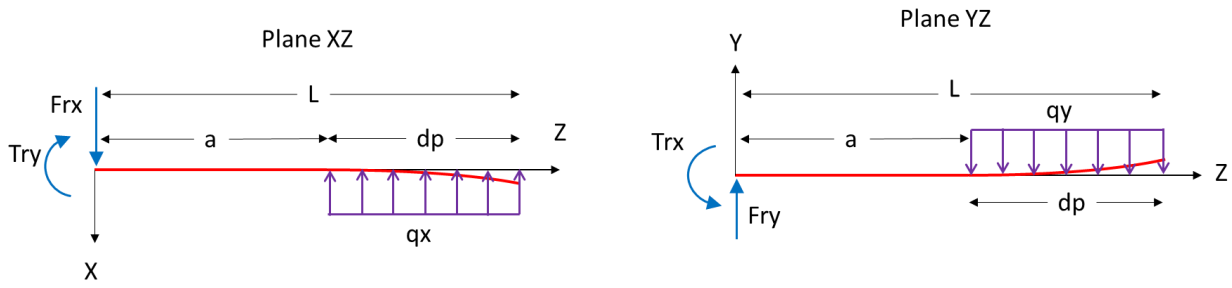

Figure 22. Model 1: Loads acting on the needle in vertical (XZ) and horizontal (YZ) planes.

For a cantilever beam subject to this type of uniform load distribution of intensity q the formula for deflection for $a \leq z \leq L$ is:

$$v_q(z) = \frac{q}{24EI}(z^4 - 4Lz^3 + 6L^2z^2 - 4a^3z + a^4) \qquad \text{(Eq.2)}$$

From this formula, deflection of the needle tip can be expressed as follows, where the load value q has the sign implicit and deflection has the same sign as the load:

$$v_q(z = L) = \delta_q = \frac{q}{24EI}(3L^4 - 4a^3L + a^4) \qquad \text{(Eq.3)}$$

The force intensity value q is calculated from the force and moment equilibrium equations. For a generic plane these are:

$$\sum \overrightarrow{F} = 0 \quad \rightarrow \quad \overrightarrow{Fr} + \vec{q}.d_p = 0 \qquad \text{(Eq.4)}$$

$$\sum \overrightarrow{M} = 0 \quad \rightarrow \quad \overrightarrow{Tr} + \vec{q}\,.d_p.\left(L - \frac{d_p}{2}\right) = 0 \qquad \text{(Eq.5)}$$

Forces and moments are considered as vectors, with their sign implicit. For Model 1, this is an overdetermined system of equations, since there is only one unknown, which is the intensity force. It is possible to solve the system and find the value of q by using an ordinary least squares method:

$$\begin{bmatrix} d_p \\ d_p.\left(L - \frac{d_p}{2}\right) \end{bmatrix} \vec{q} = \begin{bmatrix} -\overrightarrow{Fr} \\ -\overrightarrow{Tr} \end{bmatrix} \rightarrow \quad A.\vec{q} = b \rightarrow \quad \vec{q} = (A^TA)^{-1}A^Tb \qquad \text{(Eq.6)}$$

This process was equally applied to both planes, XZ and YZ, obtaining first *qx* and *qy* force intensity values from reaction forces at the base (Eq. 6) and then substituting these values in the tip deflection equation (Eq. 3) to obtain δ_{qx} and δ_{qy}.

Model 2: Uniform load distribution and point force at the tip

This variant considers a single-point force acting on the tip of the needle in addition to the uniform load distribution along the inserted portion of the needle. This single point force results from unbalance of the tissue cutting forces acting around the tip of the needle and is called *Ftx* for deflection along X axis

and *Fty* for deflection along Y axis (Figure 23). This combination of loads was also applied by Lehman (2015 & 2016-(1)) to beveled tip needles.

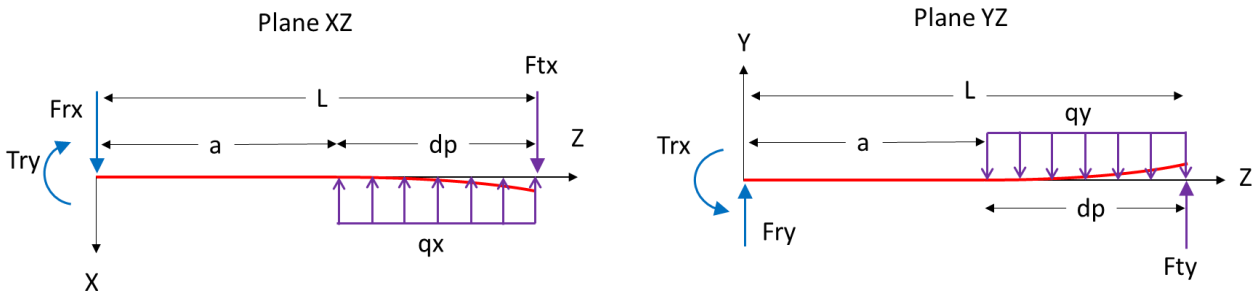

Figure 23. Model 2: Loads acting on the needle in vertical (XZ) and horizontal (YZ) planes.

In this case, deflection of the needle can be obtained by applying the superposition method explained above For a generic plane, total deflection is the sum of the deflections due to the uniform load distribution q and the point load force *Ft*:

$$v_{Tot}(z) = v_q(z) + v_{Ft}(z) \qquad \text{(Eq.7)}$$

The formula for deflection for a cantilever beam under a point force *F* at the tip is:

$$v_{Ft}(z) = \frac{F_t z^2}{6EI}(3L - z) \qquad \text{(Eq.8)}$$

From this formula, the deflection value of the needle tip due to this point load can be calculated as below, where deflection has the same sign as the force *Ft:*

$$v_{Ft}(z = L) = \delta_{Ft} = \frac{F_t L^3}{3EI} \qquad \text{(Eq.9)}$$

Applying the superposition method the resultant deflection at the tip of the needle can be expressed:

$$\delta_{Tot} = \delta_q + \delta_F = \frac{q}{24EI}(3L^4 - 4a^3L + a^4) + \frac{F_t L^3}{3EI} \qquad \text{(Eq.10)}$$

The force intensity value q and point load at the tip *Ft* can be calculated from the force and moment equilibrium equations. Considering forces and moments as vectors, with their sign implicit, the equations for a generic plane can be expressed:

$$\sum \overrightarrow{F} = 0 \quad \rightarrow \quad \overrightarrow{Fr} + \vec{q}.d_p + \overrightarrow{Ft} = 0 \qquad \text{(Eq.11)}$$

$$\sum \overrightarrow{M} = 0 \quad \rightarrow \quad \overrightarrow{Tr} + \vec{q}\,.d_p.\left(L - \frac{d_p}{2}\right) + \overrightarrow{Ft}.L = 0 \qquad \text{(Eq.12)}$$

This is a linear determinate system which can be solved to obtain the values of q and *Ft* as a function of the reaction loads and rest of parameters:

$$\overrightarrow{Ft} = \frac{(\overrightarrow{Fr}.(2L - d_p) - 2.\overrightarrow{Tr})}{d_p} \qquad \vec{q} = \frac{2}{d_p^2}.(\overrightarrow{Tr} - \overrightarrow{Fr}.L) \qquad \text{(Eqs.13 \& 14)}$$

Model 3: Uniform load distribution and Triangular load distribution

This option considers two load distributions along the inserted portion of the needle: a uniform load and a triangular load distribution. The addition of the triangular profile is expected to provide a better approximation of the real needle-tissue interaction forces compared to a simple uniform load distribution. This load combination was also applied by Lehman (2016-(1)) to estimate the deflection of beveled tip needles. The uniform force intensity will be called *q0* whereas the maximum force intensity of the triangular distribution will be called *q1* (adding x or y subscript according to the plane under analysis). Figure 24 shows a possible representation for the load distributions; the sign of each load profile could change along the insertion depending on the value and sign of the reaction forces and moments at the needle base.

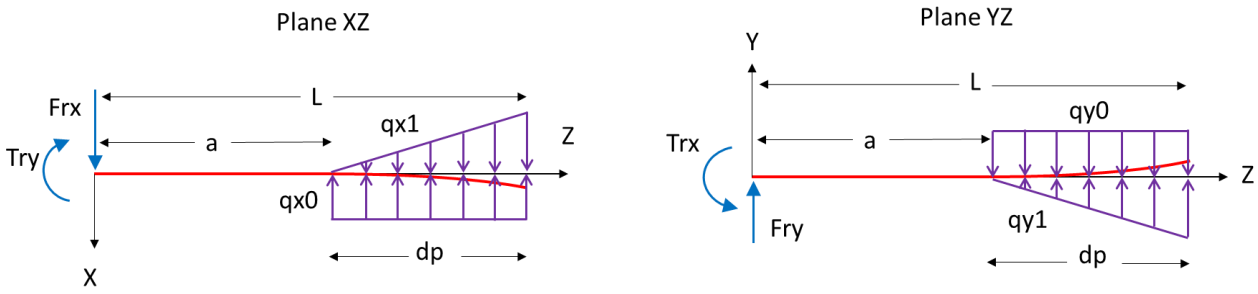

Figure 24. Model 3: Loads acting on the needle in vertical (XZ) and horizontal (YZ) planes.

As in 'Model 2', the superposition principle can be applied to calculate the total deflection of the needle as the sum of deflections due to the uniform and the triangular load distributions:

$$v_{Tot}(z) = v_{q0}(z) + v_{q1}(z) \qquad \text{(Eq.15)}$$

For the uniform load distribution the same formula described for 'Model 1' applies (Eq.2). In the case of the triangular force distribution, the expression for needle deflection was derived by double integration of the bending moment equation (Eq.1) since the formula was not available from engineering books. The calculation of this deflection equation is explained in **Appendix 3**.

$$v_{q1}(z) = \frac{q1}{120EId_p}[(z-a)^5 - 10d_p^2z^3 + 10d_p^2(2L+a)z^2] \qquad \text{(Eq.16)}$$

The tip deflection of the needle due to the triangular force distribution can then be expressed:

$$v_{q1}(z=L) = \delta_{q1} = \frac{q1.d_p}{120EI}(d_p^3 + 10L^3 + 10aL^2) \qquad \text{(Eq.17)}$$

Finally, applying the superposition method, the resultant deflection at the tip of the needle for 'Model 3' can be obtained from the sum of Eq.3 and Eq. 16:

$$\delta_{Tot} = \delta_{q0} + \delta_{q1} = \frac{q0}{24EI}(3L^4 - 4a^3L + a^4) + \frac{q1.d_p}{120EI}(d_p^3 + 10L^3 + 10aL^2) \qquad \text{(Eq.18)}$$

The force intensity values *q0* and *q1* can be obtained from the force and moment equilibrium equations. Considering forces and moments as vectors, with their sign implicit, the equations for a generic plane can be expressed:

$$\sum \overrightarrow{F} = 0 \quad \rightarrow \quad \overrightarrow{Fr} + \overrightarrow{q_0}.d_p + \overrightarrow{q_1}.\frac{d_p}{2} = 0 \qquad \text{(Eq.19)}$$

$$\sum \overrightarrow{M} = 0 \quad \rightarrow \quad \overrightarrow{Tr} + \overrightarrow{q_0}.d_p.\left(L - \frac{d_p}{2}\right) + \overrightarrow{q_1}.\frac{d_p}{2}\left(L - \frac{d_p}{3}\right) = 0 \qquad \text{(Eq.20)}$$

The solution of this linear system gives the values of *q0* and *q1* as a function of the reaction loads and rest of parameters:

$$\overrightarrow{q_0} = \frac{-2.\overrightarrow{Fr}.(3L - d_p) + 6.\overrightarrow{Tr}}{d_p^2} \qquad \overrightarrow{q_1} = \frac{6.\overrightarrow{Fr}.(2L - d_p) - 12.\overrightarrow{Tr}}{d_p^2} \qquad \text{(Eq.21)}$$

Substituting *q0* and *q1* and rest of parameters in Eq.18, total tip deflection is obtained. The same process is applied to both planes XZ and YZ.

3.2.2. Selection and evaluation of final model

The three proposed model variants were compared with regard to their prediction errors. For each needle insertion test performed in the study, actual needle tip deflection in both planes was measured at four insertion depths: 25mm, 50mm, 75mm and final depth (97mm). The three models were applied to each test; estimating needle tip deflection along full insertion depth with the equations described in section 3.2.1. Model predicted deflections at the four selected insertion points were extracted and absolute prediction errors for each model at these insertion points were calculated as the absolute differences between predicted and measured deflection values.

Performance of the models was compared separately on each plane in order to identify the best possible combination for 3D deflection estimations. The following variables were considered for the comparative analysis of the models:

- **Absolute deflection errors at final insertion depth** along X-axis and Y-axis.
- **Average absolute deflection errors per insertion test** along X-axis and Y-axis. This is the mean value of the errors in the four selected insertion depths.

First, a descriptive statistical analysis was carried out to explore the differences between the three model variants on the mean and STD of selected error variables. Second, a *Repeated Measures Analysis of Variance* was carried out to determine if there were statistically significant differences in the performance of the proposed models. From this comparative statistical analysis of prediction errors, the model variant with the lowest mean errors was selected for each plane. The final deflection estimation model was defined as the combination of the model variants with best performance in each plane.

The reliability of the selected model for estimation of needle deflection in symmetric tip needles was assessed through a *two-sample T-Test* between predicted and measured (ground truth) deflection values in both planes. This test verifies whether the means of the measured and estimated deflections are equal. In the case that equality of means cannot be rejected, the model could be considered reliable for needle deflection prediction. The variables considered for this analysis were the measured needle tip deflection values along X-axis and Y-axis at insertion depths of 25mm, 50mm, 75mm and final insertion (97mm); as well as the mating predicted deflection values resulting from the final model. For a more detailed analysis of the model's performance data were split into groups resulting from the possible combinations of needle type, tissue stiffness, skin layer and insertion depth. This allowed investigating how model performance is affected by different conditions and identifying those with higher prediction reliability.

The statistical analysis for comparison of different model variants and subsequent evaluation of the reliability of the selected model was carried out with *Matlab 2017b (Statistics and Machine Learning Toolbox).*

3.3. Conclusion

Regarding the experimental part of the study, this chapter has covered the technical description of the experimental setup to perform needle insertion tests into soft tissue. The ground truth method used to measure actual needle tip deflection in two planes using optical tracking has also been explained. The experiment design to investigate the influence of needle type, tissue hardness, skin layer and insertion speed on deflection behaviour, together with the statistical method for the evaluation of the level of influence of each factor have been detailed. In the next chapter, results from this statistical analysis will be reported, identifying which factors have a significant influence on the amount of needle deflection and assessing the effect of those factors and their interactions.

Concerning the deflection estimation model, three model variants based on beam-theory have been proposed and the equations for needle tip deflection have been derived for each case. The methodology for the selection of the final model from a comparative performance analysis of the proposed variants has been explained; as well as the statistical method for reliability assessment of the final model. Statistical results leading to the selection of the final model are presented in the next chapter; followed by a reliability analysis of the model, identifying those conditions where model predictions are comparable to ground truth measurements.

4. Results

4.1. Experimental evaluation of symmetric needles deflection behaviour

The influence of needle type, tissue hardness, skin layer and insertion speed on needle deflection behaviour was assessed through statistical analysis of the differences between sample groups resulting from various test conditions with regard to three variables describing needle tip deflection:

- Final deflection along X-axis (dx_end); this quantifies both, deflection amount and direction.
- Final deflection along Y-axis (dy_end); also quantifies deflection amount and direction.
- Final absolute deflection (dt_end) or amount of total deflection.

The influence of each factor on these variables was first explored through box-plots and comparison of mean and STD values of different groups within each factor.

Needle type

Descriptive statistics show larger average deflections for plastic needles, mainly along X-axis (vertical). Plastic needles generally show a larger variability in their behaviour compared to Titanium needles, reflected by larger STDs (Table 2 and Figure 25). Plastic needles show a tendency to downwards deflection (positive X-axis) whereas Titanium needles show a relatively symmetric deflection behaviour both in X and Y axes.

Needle	**Mean ± STD (mm)**		
	dx_end	**dy_end**	**dt_end**
Plastic	1.86 ± 1.26	0.28 ± 1.58	2.53 ± 1.06
Titanium	0.08 ± 1.10	-0.41 ± 0.85	1.28 ± 0.65

Table 2. Summary statistics of final needle deflection variables grouped by needle type.

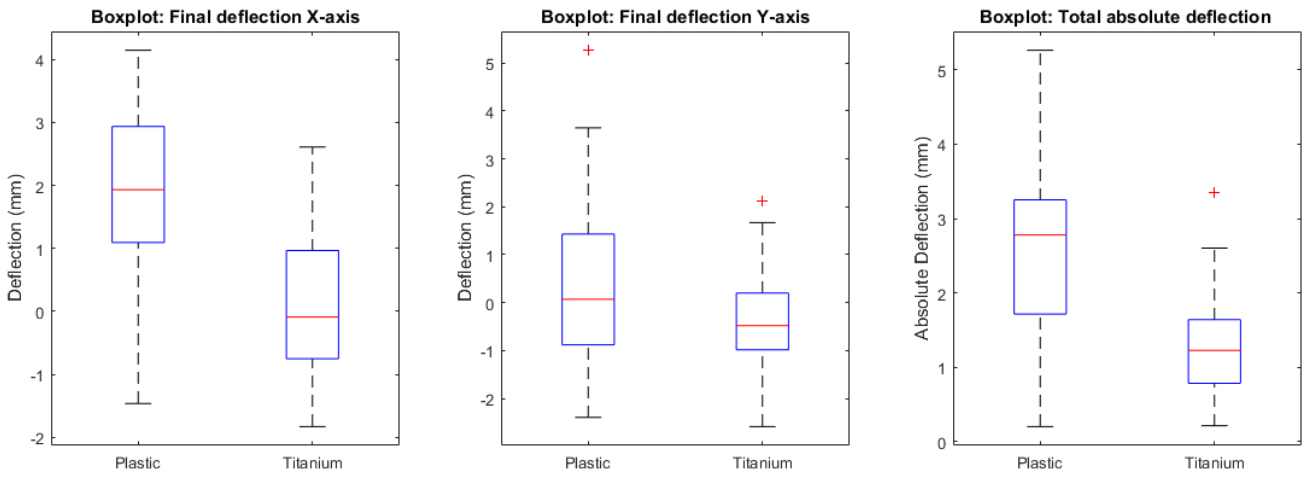

Figure 25. Box-plots of final deflection variables grouped by type of needle.

Tissue hardness

To explore this effect only samples without skin layer were considered, since the lowest density was only tested without skin and mixing skin and no-skin data could mislead the interpretation of results. Average needle deflection along X-axis is higher for intermediate tissue density (10%) (Table 3). However, there is no clear influence of tissue density on deflection along Y-axis based on the mean and STD values and the box-plot representation (Figure 26). A clearer effect of tissue hardness can be noticed on total absolute needle deflection, with deflection rising with increasing tissue density.

Tissue density	Mean ± STD (mm)		
	dx_end	dy_end	dt_end
5%	0.46 ± 1.10	-0.41 ± 0.73	1.19 ± 0.81
10%	1.32 ± 1.53	-0.30 ± 1.03	1.98 ± 1.10
20%	0.62 ± 1.84	-0.06 ± 1.66	2.29 ± 1.03

Table 3. Summary statistics of final needle deflection variables grouped by tissue density.

Figure 26. Box-plots of final deflection variables grouped by tissue density (proportional to hardness).

Skin vs. No skin

Only data from tissue densities 10% and 20% were explored, since 5% density was only tested without skin. The addition of a skin layer seems to have a certain influence on the vertical deflection along X-axis, since both, mean and median deflections are higher in those tests samples with the skin layer. However, no clear difference is observed between both groups for deflection along Y-axis (Table 4). Mean total absolute deflections are very similar between both groups, although the median of the samples with skin layer is higher compared to the samples with no skin (box-plot in Figure 27).

Skin	Mean ± STD (mm)		
	dx_end	dy_end	dt_end
With skin	1.27 ± 1.35	0.21 ± 1.44	2.08 ± 1.09
No skin	0.96 ± 1.71	-0.18 ± 1.38	2.14 ± 1.06

Table 4. Summary statistics of final needle deflection variables grouped by use of skin layer.

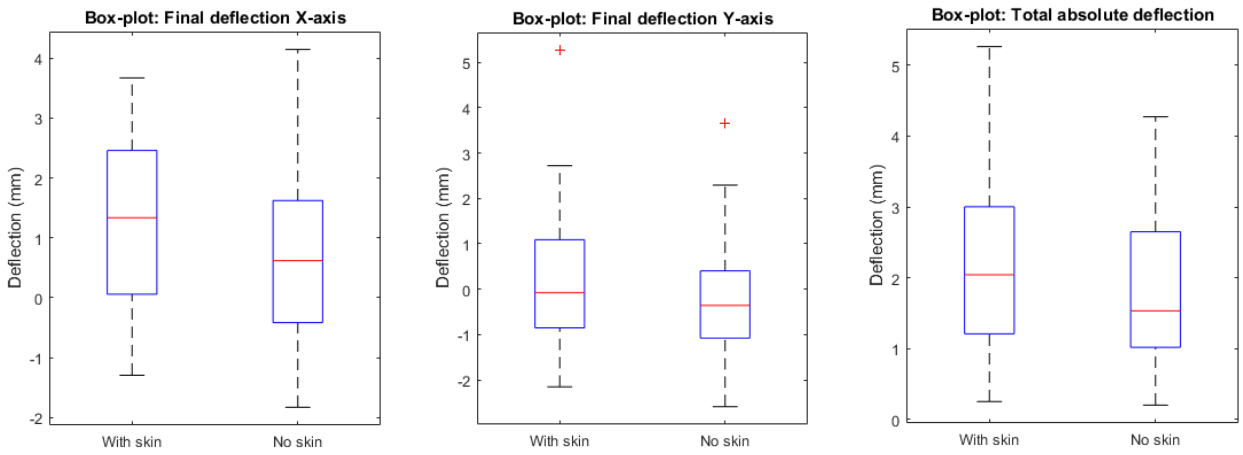

Figure 27. Box-plots of final deflection variables grouped by use of skin layer or not.

Insertion speed:

Descriptive statistics comparing low and high insertion speed levels do not show an evident influence of this factor in the needle tip deflection. No clear differences can be observed between both groups for any of the deflection variables under analysis (Table 5 & Figure 28).

Skin	**Mean ± STD (mm)**		
	dx_end	**dy_end**	**dt_end**
Low	0.90 ± 1.39	-0.23 ± 1.42	1.88 ± 1.11
High	1.09 ± 1.56	0.12 ± 1.20	1.98 ± 1.07

Table 5. Summary statistics of final needle deflection variables grouped by insertion speed.

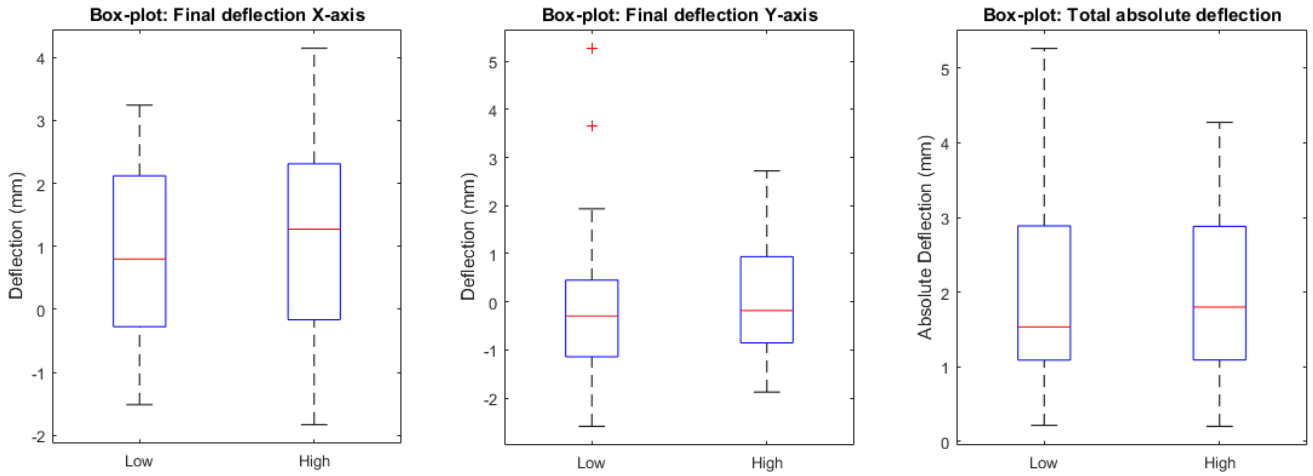

Figure 28. Box-plots of final deflection variables grouped by tested speed levels.

Combined effects were explored through comparison among groups resulting from all possible combinations of the four factors under analysis. Summary statistics of tip deflection variables for every group as well as corresponding box-plots are included in **Appendix 4**. Results show that the combination of **plastic needles with the hardest tissue and skin layer yields the largest absolute deflections**; whereas titanium needles produce the lowest absolute deflection values. Although

differences among different tissue densities can be observed (Figure 29), a clear trend with regard to tissue stiffness and use of skin cannot be easily distinguished.

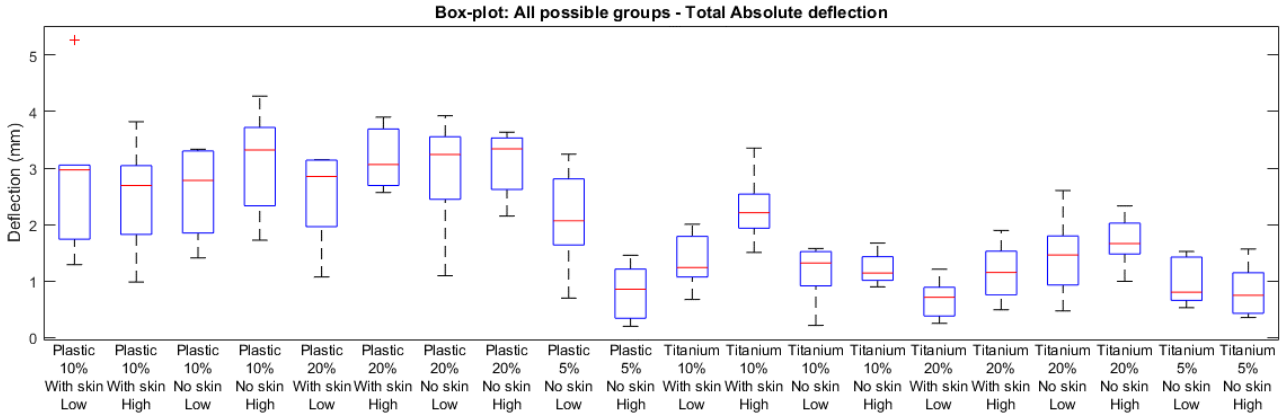

Figure 29. Box-plot of final total absolute deflection grouped by all possible factor combinations.

Multi-way Analysis of Variance (ANOVA) was carried out to assess the statistical significance of the influence of the different factors on needle deflection. ANOVA tests were applied to the three final tip deflection variables after previous assessment of normality using *Kolmogorov-Smirnov* test and homogeneity of variance across sample groups using *Levene's* test (results in **Appendix 5**). Deflection along Y-axis and absolute total deflection do not meet the normality condition but all the three variables pass the *Levene's* test for homogeneity of variance across sample groups. Application of ANOVA in this scenario is still acceptable; nevertheless, in order to contrast the findings, non-parametric *Kruskal-Wallis* tests were also performed for the evaluation of factor effects.

	Multi-way ANOVAs p-values		
Factor / Interaction	**dx_end**	**dy_end**	**dt_end**
Needle Type	< 0.001 ***	< 0.05 *	< 0.001 ***
Tissue hardness (density)	< 0.01 **	> 0.1	< 0.001 ***
Skin	> 0.1	> 0.1	> 0.1
Insertion speed	> 0.1	> 0.1	> 0.1
Needle:Tissue	< 0.001 ***	< 0.05 *	< 0.05 *
Needle:Skin	< 0.05 *	< 0.05 *	> 0.1
Needle:Speed	> 0.1	> 0.1	> 0.1
Tissue:Skin	> 0.1	< 0.05 *	< 0.1
Tissue:Speed	> 0.1	> 0.1	< 0.1
Skin:Speed	> 0.1	> 0.1	> 0.1

Table 6. Results from multi-way ANOVAs including two-factor interactions. Factors and interactions with p-value < 0.05 are marked in green.

Results from each ANOVA test including two-factor interactions are included in **Appendix 5** and summarized in Table 6. Needle type and tissue hardness have a statistically significant effect on needle deflection behaviour. In contrast, neither the addition of a skin layer nor the insertion speed have a significant influence on any of the deflection variables under analysis. Needle type significantly affects all deflection variables, whereas tissue density mainly affects deflection along X-axis and total absolute

deflection. Plastic needles suffer a significantly larger deflection than titanium needles, mainly along vertical X-axis (mean differences in Figure 30). Absolute mean deflection values along Y-axis are similar between both types of needle, although they have different predominant bending directions.

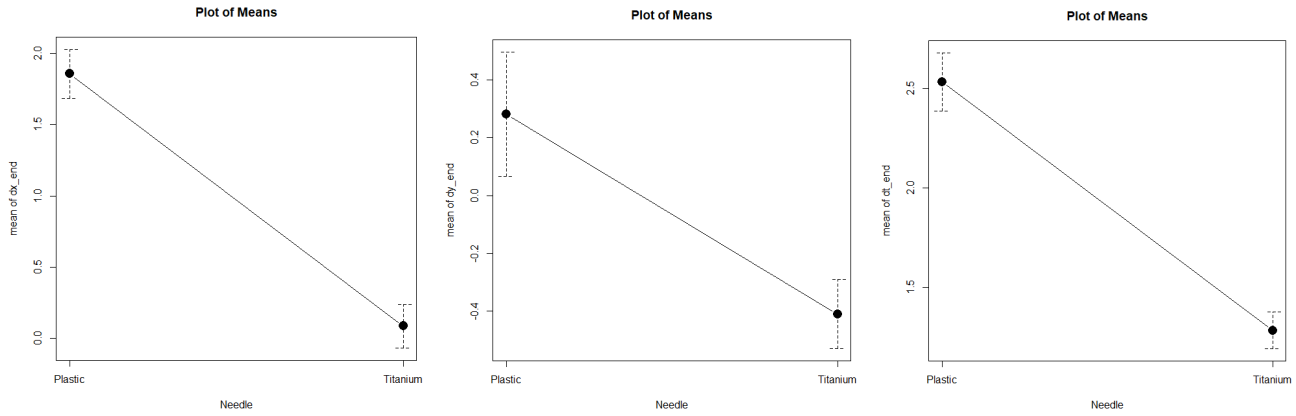

*Figure 30. Plots of means for tip deflection variables showing the effect of **Needle type**. From left to right: deflection along X-axis, Y-axis and total absolute deflection.*

Total absolute deflection increases with tissue hardness, although this trend is non-linear (Figure 31). Tukey contrast tests identified a significantly lower deflection for the 5% density group compared to 10% and 20% densities but no significant differences between the latter. In contrast, multiple comparison of deflections along X-axis resulted in 10% density producing significantly larger values than the other two groups (Appendix 5).

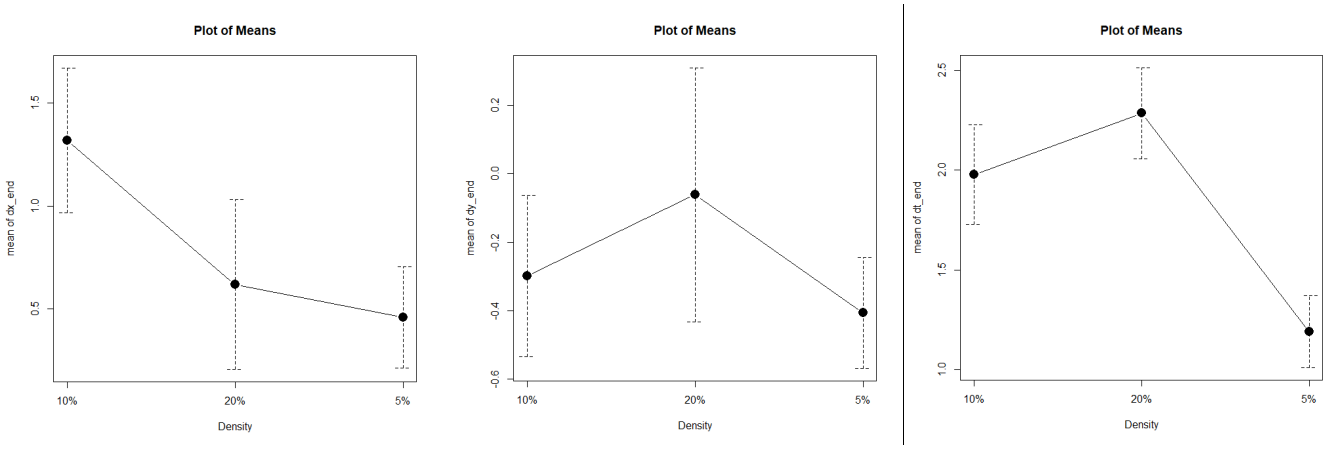

*Figure 31. Plots of means for tip deflection variables showing the effect of **Tissue hardness**. From left to right: deflection along X-axis, Y-axis and total absolute deflection.*

Significant interactions exist between needle type and tissue hardness and between needle type and the skin layer; meaning that tissue stiffness and the addition of the skin layer produce different effects depending on the type of needle. Plots in Figure 32 and Figure 33 show these interaction effects. Plastic needles behaviour is more sensitive to changes of tissue hardness than that of titanium needles. Both needles show an increasing trend for total absolute deflection with tissue hardness, but different

behaviours are observed on X and Y deflection components. Plastic needles always have a downwards deflection with the largest values for 10% tissue density and lowest values for 5% density; whereas titanium needles also experience upward deflection and have larger absolute deflection values for 20% tissue densities, with very little difference between 5% and 10% tissue densities. With regard to deflection along Y-axis, both types of needles have their largest absolute deflections for 20% tissue density.

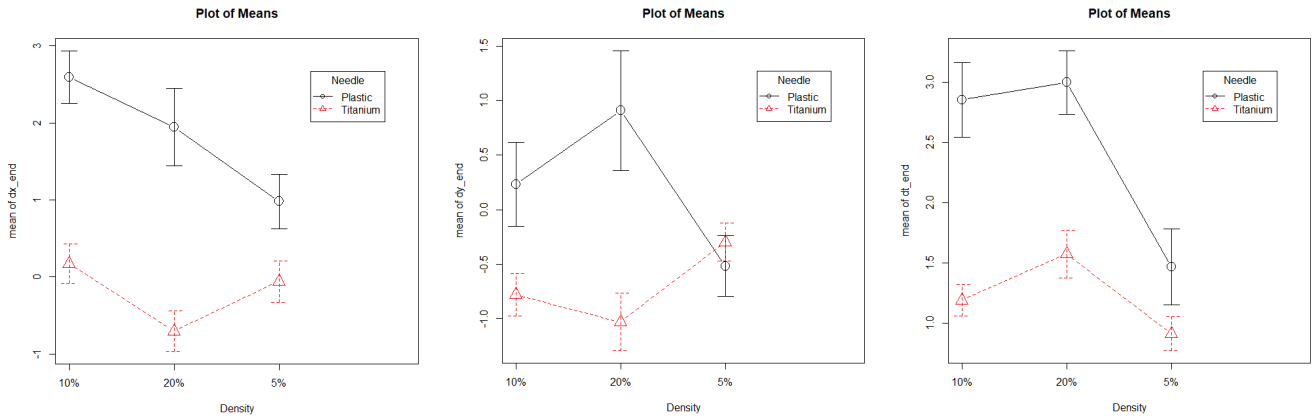

*Figure 32. Plots of means for tip deflection variables showing the **interaction between Needle type & Tissue density**. From left to right: deflection along X-axis, Y-axis and total absolute deflection.*

The addition of a skin layer only has a significant interaction effect on X and Y deflection components. This effect is more noticeable on titanium needles, which suffer larger variation of the mean deflection than plastic needles. However, in terms of absolute total deflection, the addition of a skin layer doesn't produce significant changes on the average values in any of the needles (Figure 33).

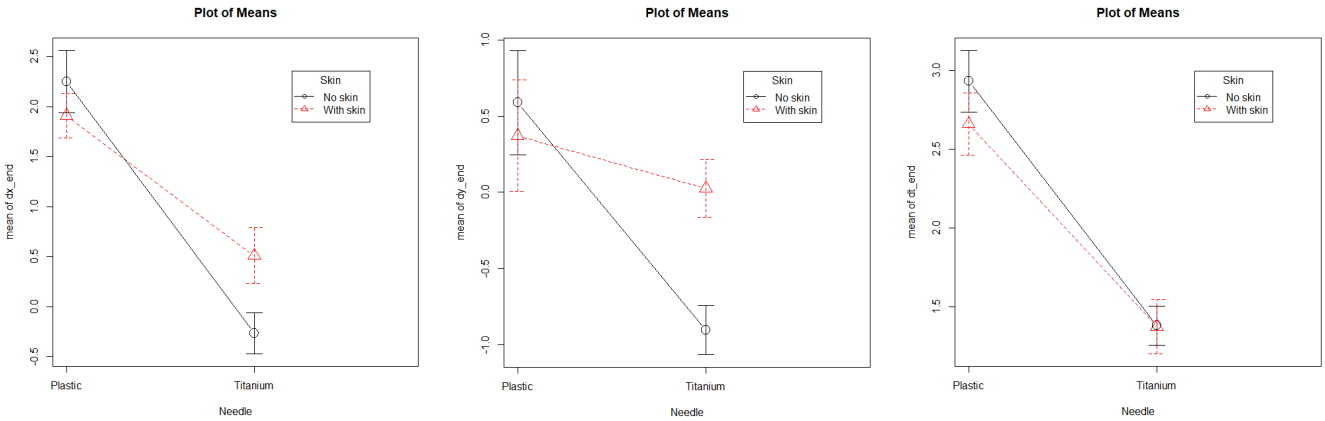

*Figure 33. Plots of means for tip deflection variables showing the **interaction between Needle type & Skin**. From left to right: deflection along X-axis, Y-axis and total absolute deflection.*

Results from non-parametric *Kruskal-Wallis* tests are totally consistent with the previous ANOVA results with regard to the influence of the main factors. Individual results from these tests are summarized at the end of **Appendix 5**.

4.2. Evaluation of proposed deflection model

4.2.1. Selection of best model approach

For each insertion test performed in the study, needle tip deflection along the full insertion depth was estimated with every proposed model variant. Figure 34 shows one example of these predicted deflections including the actual measured deflection values at four specific insertion depths for comparison. For every insertion test, absolute prediction errors were calculated for each model variant at those specific insertion depths.

As explained in section 3.2.2., the three proposed deflection models were compared with regard to their mean absolute prediction errors in each plane. These were quantified by two different variables:

- Absolute deflection errors at final insertion depth.
- Average absolute deflection errors per insertion test.

Table 7 shows the mean and STD values of the overall prediction errors for each model. Model 1 has the lowest mean prediction error along Y-axis (horizontal deflection), but the highest mean prediction error along X-axis (vertical deflection), both for the deflection at the final insertion depth and for the average prediction along the insertion depth. Models 2 and 3 perform better for estimating needle deflection along X-axis, with Model 2 having lower mean error values. However, it is difficult to tell if one of these two models is better than the other since their prediction errors are quite similar.

Model	Absolute prediction errors at final insertion depth (mm)		Average absolute prediction errors along insertion depth (mm)	
	X-axis	Y-axis	X-axis	Y-axis
1	3.88 ± 3.53	5.29 ± 4.25	2.37 ± 2.20	3.66 ± 2.98
2	2.06 ± 2.13	8.94 ± 6.00	1.31 ± 1.19	6.00 ± 4.42
3	2.15 ± 2.22	8.66 ± 5.83	1.34 ±1.23	5.88 ± 4.35

Table 7. Summary of mean and STD of prediction errors for all insertion tests for each model variant. Lowest mean errors are marked in green.

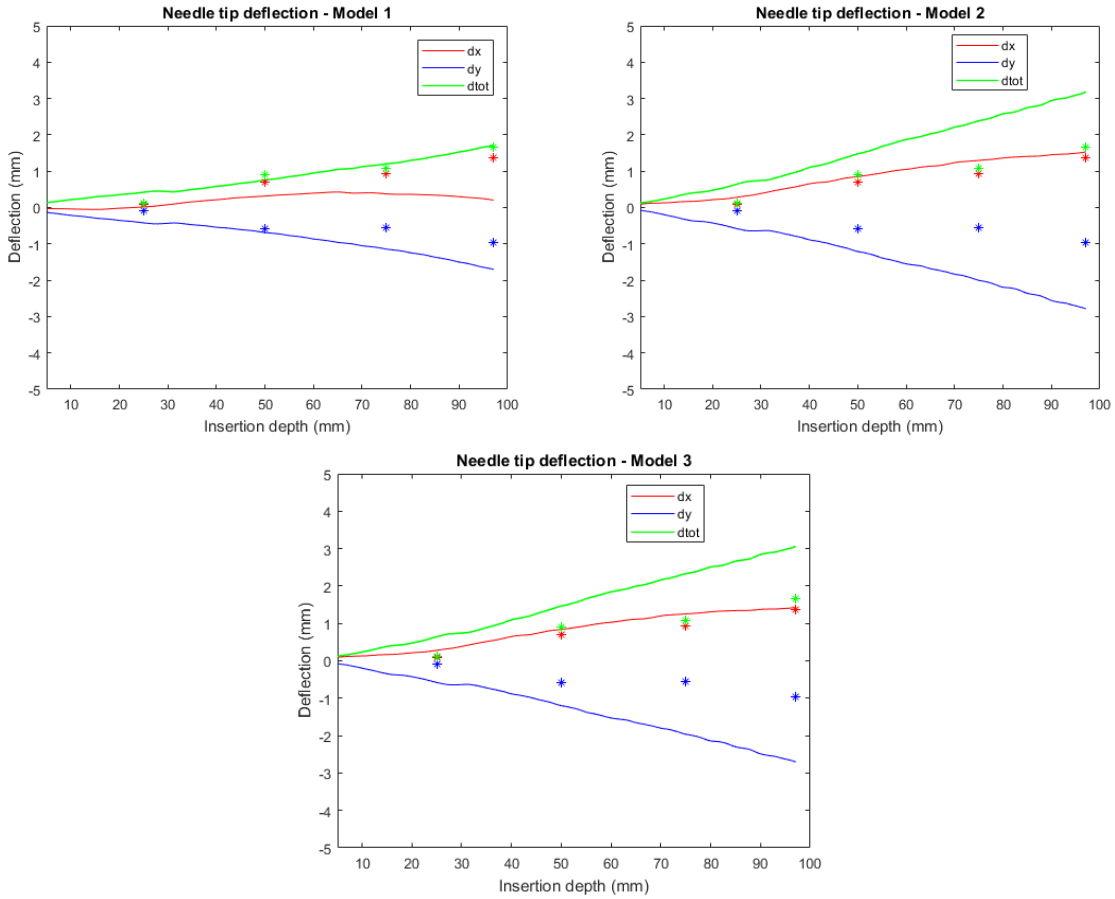

Figure 34. Needle tip deflection predictions along the insertion depth by the three proposed models for one of the insertion tests (Titanium needle, 10% tissue density with no skin). Continuous lines represent model predicted deflection values along X-axis (red), Y-axis (blue) and total absolute deflection (green). Star points represent the actual measured deflection values at specific insertion depths (25mm, 50mm, 75mm and final).

A *Repeated Measures Analysis of Variance* (ANOVA) with pair-wise comparisons using *Tukey-Kramer* test was carried out in order to determine if there were statistically significant differences in the performance of the proposed models and particularly, between Models 2 and 3. Results from this analysis are included in **Appendix 6** and show that all models are significantly different from each other with regard to their mean absolute prediction errors.

Performance of the models differs depending on the plane considered for deflection estimation. Model 1 gives the best performance for deflection prediction along Y-axis, whereas Model 2 gives the lowest mean absolute prediction errors in X-axis. Therefore, the **most suitable model for prediction of 3D deflection of the symmetric needles used in this study is a combination of Model 2 for X-axis and Model 1 for Y-axis**. The resulting model is characterized by a uniform load distribution along the inserted portion of the needle in both planes XZ and YZ, together with a single-point force acting on the tip of the needle along X-axis (Figure 35).

For most of the needle insertion tests performed in this study, a consistently different needle deflection behaviour has been observed between XZ (vertical) and YZ (horizontal) planes. Absolute vertical

deflection value (X-axis) is generally larger than horizontal deflection (Y-axis). This different behaviour explains why different load profiles are needed for each plane. On YZ plane, average deflection values are quite small, so the addition of a point load at the tip would result in overestimation of the deflection value. In contrast, on XZ plane where deflections are larger, a uniform load distribution is not enough to produce the actual amount of deflection observed along X-axis.

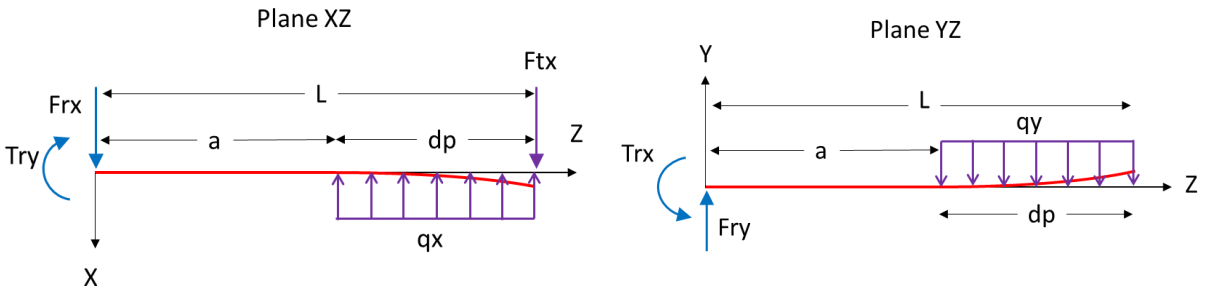

Figure 35. Load profiles characterizing the selected final model.

4.2.2. Reliability evaluation of final selected model

Reliability of the selected model was assessed through statistical comparison of measured needle tip deflection values and those predicted by the final model. A *two-sample T-test* was performed to check the equality of means between measured and predicted deflection values along both, X and Y axes. When hypothesis for equal means cannot be rejected, reliability of the model for estimation of needle deflection is considered high, since predicted deflections are not significantly different from actual deflections. Data sample included deflection values at insertion depths of 25mm, 50mm, 75mm and final insertion (97mm) for every insertion test performed in the study. Data were split into groups resulting from the possible combinations of needle type, tissue hardness, skin layer and insertion depth. Results from these T-Tests have been included in **Appendix 7**.

This analysis shows that **reliability of the model is generally quite low for estimation of plastic needles deflection**, since model prediction is significantly different to actual needle deflection values in all the combinations except for deflection at final insertion depth in tissue samples of density 5% and deflection along X-axis in tissue density 20% with no skin.

Reliability of the model is higher for Titanium needles, although mainly for deflection predictions along X-axis. The model predicts well vertical deflection values for tissue samples with 10% density and no skin. Also, predicted deflections at final insertion depth are not significantly different from measured deflections in any of the tissue densities without skin layer. However, the model doesn't seem reliable for estimation of Y-axis deflections.

The combination of the **longest insertion depth (97mm) with the lowest tissue density of 5% with no skin** seems to be the only scenario where the **model can predict needle deflection in both planes** more reliably.

Table 8 shows the mean and STD values of final model prediction errors along the insertion depth for deflections in both planes. Data are grouped per needle type, tissue density and use of skin layer. Differences between these groups can also be observed in Figure 36.

In agreement with the previous T-test analysis, the lowest error in plastic needles is observed for the lowest tissue density, both for deflection along X and Y axes. This is a submillimetre error and according to the statistical analysis, model predictions cannot be distinguished from actual measured deflections.

Increasing tissue density or hardness, yields higher prediction errors in plastic needles, particularly for deflection along Y-axis.

The model seems to work better for metal needles, with submillimetre average errors in X-axis for all the group combinations and for 'non-skin' 5% and 10% tissue densities in Y-axis deflection. Increasing tissue hardness also has a negative effect on model's performance, although it is not as sound as for plastic needles.

The addition of a skin layer increases the model prediction errors significantly in both types of needles.

According to these results, it could be said that **the proposed model doesn't work for prediction of needle deflection into multiple-layer tissue nor for harder tissue**. The model works better for titanium than for plastic needles, indicating that **model predictions improve with stiffer needle material**.

Needle	Density	Skin	Error in X (mm)	Error in Y (mm)
Plastic	5%	No Skin	0.56 ± 0.31	0.57 ± 0.36
	10%	No Skin	1.23 ± 1.03	2.18 ± 1.50
		With Skin	2.58 ± 1.47	6.82 ± 3.25
	20%	No Skin	1.18 ± 1.02	5.62 ± 2.93
		With Skin	3.14 ± 1.74	8.65 ± 2.35
Titanium	5%	No Skin	0.67 ± 0.30	0.34 ± 0.22
	10%	No Skin	0.29 ± 0.16	0.71 ± 0.52
		With Skin	0.95 ± 0.68	3.28 ± 2.00
	20%	No Skin	0.68 ± 0.43	2.47 ± 1.36
		With Skin	0.69 ± 0.49	4.57 ± 1.94

Table 8. Mean and STD of model prediction errors in both planes. Combination with submillimetre errors in both axes are colour-marked.

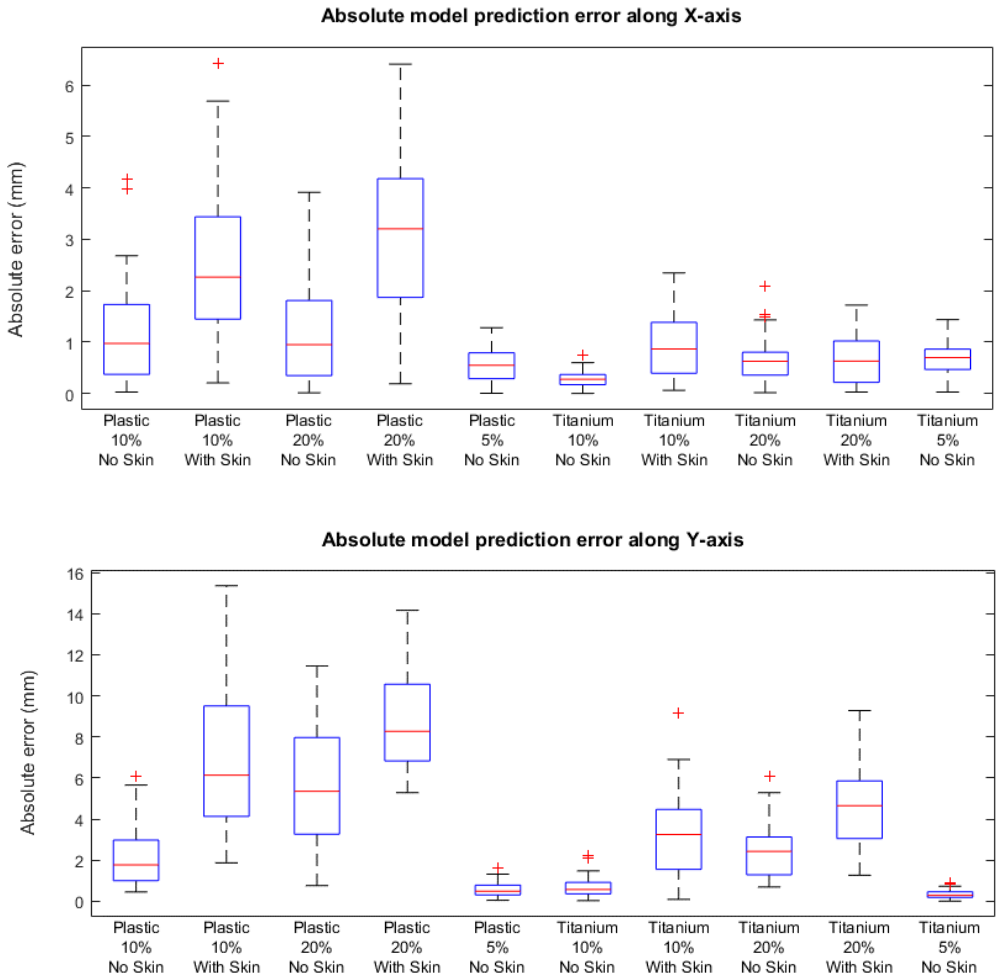

Figure 36. Box-plots of model prediction errors in both planes grouped per needle type, tissue density and use of skin layer.

5. Discussion

Two main research objectives have been addressed by this study. A first goal was to investigate how certain factors affect deflection behaviour of brachytherapy symmetric tip needles when inserted into soft tissue. The second target was to develop an analytical model for deflection prediction of symmetric brachytherapy needles from reaction forces measured at the base of the needle and evaluate the performance of this model with experimental data.

In the previous chapter, the influence of needle type, tissue hardness, skin layer and insertion speed parameters on needle tip deflection at the final insertion depth was investigated through statistical analysis of deflection data measured at all needle insertion tests performed in the study. Likewise, a final version of the model for deflection prediction was defined after a comparative performance analysis of the three model variants initially proposed. Finally, reliability of this model was statistically evaluated, identifying those conditions where model predictions are comparable to ground truth measurements. Discussion and analysis of the research findings has been split into two sections that specifically respond to each research objective.

5.1. Experimental evaluation of symmetric needles deflection behaviour

Symmetric brachytherapy needles tested in this study experienced small deflections with mean values of total absolute tip deflections equal to 1.28 ± 0.65mm for titanium needles and 2.53 ± 1.06 mm for plastic needles at 97mm insertion depth. These deflection values are similar to those reported by other authors for symmetric brachytherapy needles with diamond and conical tip geometries respectively (Podder, 2005; van Veen, 2012; De Jong, 2015).

The combination of plastic needles with the highest tissue hardness (20% density) produced the largest total absolute deflection values (2.89±0.82mm). In contrast, titanium needles with the lowest tissue hardness (5% density) yield the lowest absolute deflections (0.91±0.44 mm).

Assuming a perfect initial alignment of the needle axis with the insertion trajectory, deflection behaviour of symmetric needles inserted into homogeneous tissue should be comparable between vertical and horizontal planes. However, deflection of plastic needles in the current study is biased to the vertical plane, with predominantly downwards deflection. This is due to the decision to place plastic needles so that initial deflection before insertion was always positive along X-axis. As mentioned in the methodology chapter, all plastic needles had a certain default curvature which resulted in a tip deviation from the insertion axis that could be larger than 1mm. It is believed this is caused by residual stresses on the needle due to the manufacturing process. In order to isolate the effect of this initial deflection bias and make final results more comparable, all tested plastic needles were placed so that their inherent curvature was constrained to the vertical plane (XZ) and their tip pointed downwards. Final deflection

results clearly show the influence of this initial vertical deflection bias, since deflections along X-axis are mostly positive whilst deflections along Y-axis have a random behaviour with average values close to zero. Titanium needles have tighter angularity tolerances on their axis and it is almost perpendicular to the needle base; this minimizes any bias effect due to initial deviations. Results confirm that titanium needles have a similar behaviour in both planes with a random deflection behaviour around the insertion axis.

The study reveals a significantly different behaviour between plastic and titanium needles. The initial hypothesis was that plastic needles would bend more due to their lower stiffness. Although the study shows that in effect, plastic needles bend more than titanium needles, this difference is mainly observed in the vertical plane, where plastic needles have a larger initial deflection before insertion as mentioned above. In the horizontal plane, absolute mean deflection values are similar between both types of needles (Figure 30). Therefore, the different behaviour could be caused by the inherent curvature of plastic needles, more than being due to the different materials stiffness. Further testing with plastic needles having comparable straightness and initial deviation to titanium needles should be carried out in order to confirm differences in the deflection behaviour due to needle material and tip geometry. However, it seems that the curvature defect of plastic needles is inherent to the manufacturing process (all available plastic needle samples had the same feature). If that is the case, results of this study suggest that plastic needles are less reliable for clinical application since they are more likely to produce larger targeting errors than titanium needles.

Regardless of the needle type, harder tissue samples produce larger absolute deflection values. This is consistent with previous experimental studies (Podder, 2005; van Veen, 2012; Lehmann, 2015; Lehmann, 2016-(2)) and confirms the initial hypothesis of this research. Results also show this relationship is not linearly proportional, with the lowest density (5%) producing significantly lower total absolute deflections compared to the two higher densities (10% and 20%). This can be interpreted as a reduction of the influence of tissue hardness on needle deflection with increasing hardness.

With regard to two-layer insertion effect, the initial hypothesis was that it would increase the amount of needle deflection as well as the variability of results. ANOVAs of available test data don't show a significant effect of the skin layer on mean needle deflection values. This finding also differs from the research work published by Lee (2014), who measured larger final target deviation values in two-layer phantoms compared to homogeneous samples. However, Lee's study is not directly comparable since they used thinner biopsy needles (0.8mm diameter), which are more likely to bend than brachytherapy needles. The addition of a skin layer didn't affect the variability of deflection data either. This was confirmed through *Levene's* tests for equality of variance between samples with and without skin.

Speed levels tested in this study do not produce significantly different deflection values. This is consistent with previous findings by Webster (2005) and Lehmann (2013) and the initial hypothesis,

but different to results from other studies (van Veen, 2012; McGill, 2012). It could be that the difference between average speed values selected for the study is not large enough to produce significant changes on needle deflection. Additional tests with larger differences between insertion speed values would provide further insight on the effect of this factor.

5.2. Model for estimation of needle deflection

Comparative assessment of three model variants showed that needle-tissue interaction forces fit to different profiles for vertical and horizontal deflection planes. The bias to downward deflection observed on plastic needles could be the reason why different load profiles are needed for each plane. Larger vertical deflections are better represented by a load profile including a point force at the tip of the needle, whereas small random horizontal deflections can be better explained by a uniform load distribution resulting from the unbalanced forces on both sides of the needle.

In order to confirm if the different behaviour observed for both types of needles had an effect on the selection of the final model, performance of the three model variants was compared for plastic and titanium needles. Table 9 shows prediction errors of each model variant grouped by needle type. Model 1 is still the best approach for deflection estimation along Y-axis for both needles. Regarding deflections along X-axis, Model 3 has slightly lower mean prediction errors than Model 2 for titanium needles. However, these differences are so minor that the application of Model 2 for titanium needles could still be considered acceptable.

Needle	Model	Absolute prediction errors at final insertion depth (mm)		Average absolute prediction errors along insertion depth (mm)	
		X-axis	Y-axis	X-axis	Y-axis
Plastic	1	6.25 ± 3.32	7.00 ± 4.75	3.85 ± 2.14	4.97 ± 3.31
	2	3.26 ± 2.34	11.05 ±6.60	1.93 ± 1.35	7.66 ± 4.95
	3	3.46 ±2.38	10.74 ± 6.41	2.00 ± 1.38	7.53 ± 4.86
Titanium	1	1.37 ± 1.32	3.49 ± 2.68	0.80 ± 0.62	2.27 ± 1.74
	2	0.78 ± 0.64	6.71 ± 4.34	0.65 ± 0.35	4.24 ± 2.92
	3	0.76 ± 0.63	6.46 ± 4.20	0.63 ± 0.34	4.14 ± 2.87

Table 9. Average prediction errors of three model variants grouped by type of needle. Lowest mean errors are marked in green.

The fact that the model works better to predict deflection of titanium needles is consistent with beam theory assumptions. Application of beam deflection equations is correct for rigid beams that suffer very small or negligible deflections under the application of bending loads. Mechanical behaviour of titanium and other metal brachytherapy needles responds better to this assumption than plastic needles, which are more flexible and produce larger deflections. This explains why the model has lower prediction errors for titanium needles.

To the author's knowledge, no research has been published about models for deflection estimation of symmetric tip needles. So far, research on modelling brachytherapy needles deflection behaviour has

focused on beveled tip needles, which bend significantly more than symmetric tip needles due to the asymmetric profile of needle-tissue interaction forces. This modelling preference is due to their steerability, making them suitable for robotic needle insertion systems.

The application of beam-theory modelling approach to brachytherapy metal beveled tip needles has proven an adequate performance for *in vitro* estimation of needle tip deflection during insertion into soft tissue. After trying a number of models with different profiles of needle-tissue interaction forces, Lehmann (2016-(1)) obtained the best performance with a combination of a uniform distributed load and a triangular load distribution; equivalent to the 'Model 3' variant proposed in this study. Prediction errors of Lehmann's 2D model for needle insertion into gelatine phantoms and porcine loin muscle tissue were lower than 1 mm along an insertion depth of 130mm (with final deflection values between 10mm and 15mm). Statistical comparison between model estimations and ground truth measurements resulted in no significant differences along the full insertion depth for all tested tissue samples; showing a high prediction reliability.

The application of the same beam-theory approach to symmetric titanium needles in this study resulted in mean prediction errors below 1mm for deflection along X-axis. However, estimated deflection is comparable to ground truth measurements only at the final insertion depth.

In contrast to bevel tip needles, which can bend 10mm or more for insertion depths equal or longer than 100mm, deflection of symmetric needles is really small (≤1mm). The ground truth method used to measure needle deflections has a limited accuracy and measuring errors could be larger than 0.5mm. This means that it could be possible that a significant part of the difference between measured and predicted deflection values was due to measuring errors and not to model errors.

In the proposed model, the load profile proposed for deflections along X-axis seems to be representative enough across different tissue conditions, particularly for titanium needles, were average prediction errors are all below 1mm (Table 8). However, deflection estimations along Y-axis are quite sensitive to changes of tissue hardness, with significantly larger errors for tissue density 20% in both needles. This could indicate that needle-tissue interaction forces do not fit into a uniform load distribution profile, but there must be additional interaction loads with insertion into harder tissue samples. The effect of tissue hardness on the performance of the three model variants was further investigated by comparing prediction errors for tissue samples without skin layer. Absolute model prediction errors for each needle-tissue combination are summarized in **Appendix 8**. Results show that although prediction errors along Y-axis increase with tissue hardness, Model 1 still produces the lowest errors among the three variants for all needle-tissue combinations.

As mentioned in the literature review, the main challenge to achieve accurate beam-type deflection models is to define load profiles which are representative of the actual needle-tissue interaction forces under real insertion conditions. As already pointed by Lehmann (2015), it is likely that the shape of the load profile changes throughout the insertion due to the dynamic nature of the process. However, real-

time adaptation of the shape of the interaction forces profile hasn't been considered yet in published beam-type deflection models. Identification of which load profile would be best for each needle/tissue combination at each insertion point in time is a challenging task, therefore research has tried to simplify the problem by finding those profile shapes that fit better to the observed needle deflection behaviour and minimize model prediction errors. The selected profiles are then kept fixed along the insertion process, with only the magnitude and sign of the forces being adapted in real time. The current study followed this same approach, identifying those load profiles that provide the lowest mean deflection estimation errors. The use of a fixed shape for the load profile along the needle insertion is therefore a limitation of this modelling approach.

Prediction reliability of the deflection model proposed in this study is quite low to be considered for clinical application. The model only provides accurate estimations of needle tip deflection for very soft homogeneous tissue. Human soft tissue mechanical behaviour is much more complex due to its heterogeneity and multiple layers, therefore higher prediction errors are expected for this type of model when applied to real soft tissue.

6. Conclusions

The first goal of this study was to **characterize the deflection behaviour of brachytherapy needles with symmetric tip geometry** and investigate the effect of a number of factors on needle deflection when inserted into soft tissue.

A dedicated experimental setup was designed and built to perform needle insertion tests and optically track the 3D position of the needle tip throughout the insertion. More than 100 needle insertion tests were carried out with an experiment design that combined needle type, tissue hardness, two-layer tissue and insertion speed. The influence of these factors on the final tip deflection was evaluated through statistical analysis of the measured deflection data.

Both, plastic and titanium needles experienced overall small deflection values which are consistent with previously published deflections for symmetric tip needles. Plastic needles experience a significantly larger total absolute deflection (2.53 ± 1.06 mm) than titanium needles (1.28 ± 0.65mm). However, it is not possible to conclude whether this distinct behaviour is mainly due to the different needle materials. It is possible that the typical curvature observed in plastic needles had a stronger effect on the final deflection values of plastic needles than their lower stiffness. Nevertheless, the study finding is useful from a clinical application perspective, since it shows that plastic needles are less reliable and titanium needles should be the preferred choice to improve targeting accuracy in brachytherapy procedures.

Experimental results also show that needle deflection increases with tissue hardness. This is consistent with previous research and confirms the importance of tissue mechanical properties as one of the main factors affecting the outcome of needle insertion.

Insertion into two-layer tissue samples didn't have a significant effect on needles deflection. There is a lack of experimental research on this aspect and the only study found that directly addressed the effect of multilayer insertion is not really comparable because they used flexible biopsy needles. From a clinical perspective, the findings of the current study indicate an adequate design of the tested brachytherapy needles, since their accuracy is not affected by the puncture of the skin layer.

Variation of insertion speed within the range tested in this study (10-15mm/s) doesn't have a significant influence on the magnitude of needle deflection. Although this is consistent with previous findings by some authors; it is also possible that the difference between selected speed values is not large enough to produce different deflection behaviours.

The second and **ultimate goal of this research was to develop and evaluate a model to predict 3D deflection of symmetric brachytherapy needles along insertion into soft tissue** without using image guidance. After a review of the state of the art, the analytical beam-theory approach was selected. The inputs to the model are the reaction shear forces and bending moments at the base of the needle, needle parameters (length, Young's Modulus and area moment of inertia) and the insertion depth. The contributions of the current research are the application of this modelling approach to estimate 3D

deflection of symmetric tip needles. Previous research had focused on 2D models to predict deflection of beveled tip needles in the main plane of bending.

Three model variants were initially considered; differing in the definition of the load profile characterizing needle-tissue interaction forces. The final selected model was defined as the combination of the load profiles giving the lowest mean absolute prediction errors in each deflection plane. The model is characterized by uniform load distributions along the inserted portion of the needle in both planes, together with a single-point force acting on the tip of the needle along X-axis (Figure 35).

A reliability analysis of the model showed a poor performance with harder and two-layer tissue; with prediction errors larger than 1mm. Model predictions are comparable to measured deflections in both planes only for the softest homogeneous tissue samples (5% density with no skin). Consistently with beam-theory, the model works better for stiffer titanium needles than for plastic needles.

Accuracy of the model is higher for prediction of vertical deflections (X) than for horizontal deflections (Y), both for plastic and titanium needles. This suggests that needle-tissue interaction forces in the horizontal plane have a more changeable and unpredictable profile compared to those in the vertical plane.

The proposed model is not reliable enough to be considered for clinical application, since its performance is very dependent on the mechanical properties of the tissue and it is only accurate for those conditions where deflections are so small that can be considered clinically negligible. Human soft tissue is characterized by a high heterogeneity and wide range of mechanical properties; it is expected that more heterogeneous soft tissues will produce more changes on the needle-tissue interaction forces throughout the insertion, therefore application of fixed load profile models would result in larger estimation errors. This is a limitation of current beam-theory models that consider a fixed shape profile for the needle-tissue interaction forces along the full insertion depth.

Recommendations for further research:

1. Experimental characterization of deflection behaviour

a) Perform tests with asymmetric tip needles (e.g. bevel tip) and compare deflection behaviour with symmetric needles.
b) Investigate the effect or multi-layer insertion with more than two layers of different densities.
c) Perform further tests at lower and higher speed values to confirm findings on the influence of this factor.

<u>Improvements to the test setup:</u>

- Increase image resolution of the optical tracking system. This would improve measuring accuracy of actual needle deflections. The drawback of this would be the larger memory space required for video data.

- Mechanical design could be improved to provide additional DOFs. This would be desirable when testing steerable needles, so the effect of rotation on the control of the needle trajectory could be studied.

2. Model for estimation of 3D needle deflection

a) Evaluate performance of the proposed beam-theory model for other types of needle tip geometry. It would be especially interesting to investigate performance for bevel tip needles and compare results with previous models proposed by Lehmann (2016-(1)).

b) Study the feasibility of data-driven models, like a Multilayer Perceptron Neural Network. The network could be trained with available and new experimental data. Evaluate the performance of the neural network approach comparing prediction errors with beam-theory analytical model.

References

Abolhassani, N., Patel, R. V. and Ayazi, F. (2007) 'Minimization of needle deflection in robot-assisted percutaneous therapy', *International Journal of Medical Robotics and Computer Assisted Surgery*, 3(2), pp. 140–148. (1)

Abolhassani, N., Patel, R. and Moallem, M. (2007) 'Needle insertion into soft tissue: A survey', *Medical Engineering and Physics*, 29(4), pp. 413–431. (2)

Abolhassani, N., Patel, R. and Ayazi, F. (2007) 'Effects of different insertion methods on reducing needle deflection', in *Annual International Conference of the IEEE Engineering in Medicine and Biology - Proceedings*, pp. 491–494. (3)

Chao, M.W., Grimm, P., Yaxley, J., Jagavkar, R., Ng, M. and Lawrentschuk, N. (2015) 'Brachytherapy: state-of-the-art radiotherapy in prostate cancer'. *BJU Int*, *116*(Suppl 3), pp.80-88.

Cormack, R. A., Tempany, C. M. and D'Amico, A. V. (2000) 'Optimizing target coverage by dosimetric feedback during prostate brachytherapy', *International Journal of Radiation Oncology Biology Physics*, 48(4), pp. 1245–1249.

De Jong, T., (2015). 'Needle deflection in tissue'. *Master's Thesis. Delft University of Technology.*

Gere JM., Goodno BJ. (2009) 'Mechanics of Materials', 7th Edition (SI Edition). *Cengage Learning, ©2009.* ISBN: 0495438073.

Glozman, D. and Shoham, M. (2007) 'Image-guided robotic flexible needle steering', *IEEE Transactions on Robotics*, 23(3), pp. 459–467.

Goksel, O., Dehghan, E. and Salcudean, S. E. (2009) 'Modeling and simulation of flexible needles', *Medical Engineering and Physics*, 31(9), pp. 1069–1078.

Goksel, O., Sapchuk, K. and Salcudean, S. E. (2011) 'Haptic simulator for prostate brachytherapy with simulated needle and probe interaction', *IEEE Transactions on Haptics*, 4(3), pp. 188–198.

Kataoka, H., Washio, T., Audette, M. and Mizuhara, K. (2001) 'A model for relations between needle deflection, force, and thickness on needle penetration'. In *International Conference on Medical Image Computing and Computer-Assisted Intervention* (pp. 966-974). Springer, Berlin, Heidelberg.

Lee, H. and Kim, J. (2014) 'Estimation of flexible needle deflection in layered soft tissues with different elastic moduli', *Medical and Biological Engineering and Computing*. Springer Verlag, 52(9), pp. 729–740.

Lehmann, T., Rossa, C., Usmani, N., Sloboda, R.S. and Tavakoli, M. (2016) 'A real-time estimator for needle deflection during insertion into soft tissue based on adaptive modeling of needle–tissue interactions'. *IEEE/ASME Transactions on Mechatronics*, *21*(6), pp.2601-2612. (1)

Lehmann, T., Rossa, C., Sloboda, R., Usmani, N. and Tavakoli, M. (2016) 'Needle path control during insertion in soft tissue using a force-sensor-based deflection estimator'. In *2016 IEEE International Conference on Advanced Intelligent Mechatronics (AIM)*. IEEE, pp. 1174–1179. (2)

Lehmann, T., Rossa, C., Usmani, N., Sloboda, R. and Tavakoli, M. (2015) 'A virtual sensor for needle deflection estimation during soft-tissue needle insertion'. In *2015 IEEE International Conference on Robotics and Automation (ICRA)*. IEEE, pp. 1217–1222.

Lehmann, T., Tavakoli, M., Usmani, N. and Sloboda, R. (2013) 'Force-sensor-based estimation of needle tip deflection in brachytherapy', *Journal of Sensors*, 2013. Article ID: 263153.

McGill, C.S., Schwartz, J.A., Moore, J.Z., McLaughlin, P.W. and Shih, A.J., (2012) 'Effects of insertion speed and trocar stiffness on the accuracy of needle position for brachytherapy'. *Medical physics*, *39*(4), pp.1811-1817.

Misra, S., Reed, K.B., Schafer, B.W., Ramesh, K.T. and Okamura, A.M., (2010) 'Mechanics of flexible needles robotically steered through soft tissue'. *The International journal of robotics research*, *29*(13), pp.1640-1660.

Okamura, A. M., Simone, C. and O'leary, M. D. (2004) 'Force modeling for needle insertion into soft tissue', *IEEE transactions on biomedical engineering*. IEEE, 51(10), pp. 1707–1716.

Podder, T.K., Sherman, J., Fuller, D., Messing, E.M., Rubens, D.J., Strang, J.G., Brasacchio, R.A. and Yu, Y., (2006) 'In-vivo measurement of surgical needle intervention parameters: a pilot study'. In *2006 International Conference of the IEEE Engineering in Medicine and Biology Society - Proceedings*, pp. 3652–3655.

Podder, T., Clark, D., Sherman, J., Fuller, D., Messing, E., Rubens, D., Strang, J., Zhang, Y., O'Dell, W., Ng, W. and Yu, Y., (2005) 'Effects of tip geometry of surgical needles: an assessment of force and deflection'. In *IFMBE Proc.* Vol. 11, No. 1, pp. 1727-1983.

Popescu, T., Kacsó, A.C., Pisla, D. and Kacsó, A.P.G., (2015) 'Brachytherapy next generation: robotic systems'. *Journal of contemporary brachytherapy*, *7*(6), p.510.

Ravali, G. and Manivannan, M. (2017) 'Haptic feedback in needle insertion modeling and simulation', *IEEE reviews in biomedical engineering*. IEEE, 10, pp. 63–77.

Sadjadi, H., Hashtrudi-Zaad, K. and Fichtinger, G. (2014) 'Needle deflection estimation: prostate brachytherapy phantom experiments', *International journal of computer assisted radiology and surgery*. Springer, 9(6), pp. 921–929.

van Gerwen, D. J., Dankelman, J. and van den Dobbelsteen, J. J. (2012) 'Needle-tissue interaction forces - A survey of experimental data', *Medical Engineering and Physics*, pp. 665–680.

Van Veen, Y. R. J., Jahya, A. and Misra, S. (2012) 'Macroscopic and microscopic observations of needle insertion into gels', *Proceedings of the Institution of Mechanical Engineers, Part H: Journal of Engineering in Medicine*, 226(6), pp. 441–449.

Wan, G., Wei, Z., Gardi, L., Downey, D.B. and Fenster, A., (2005) 'Brachytherapy needle deflection evaluation and correction'. *Medical physics*, *32*(4), pp.902-909.

Webster III, R.J., Kim, J.S., Cowan, N.J., Chirikjian, G.S. and Okamura, A.M., (2006) 'Nonholonomic modeling of needle steering'. *The International Journal of Robotics Research*, *25*(5-6), pp.509-525.

Webster, R. J., Memisevic, J. and Okamura, A. M. (2005) 'Design considerations for robotic needle steering', in *Proceedings - IEEE International Conference on Robotics and Automation*, pp. 3588–3594.

Appendices

Appendix 1: *Foundations of Beam Deflection Theory*

Any beam subject to shear forces and bending moments will deform into a curve known as the deflection curve of the beam (Figure 37). Beam theory defines several differential equations of this deflection curve and their associated relationships (Gere, 2009).

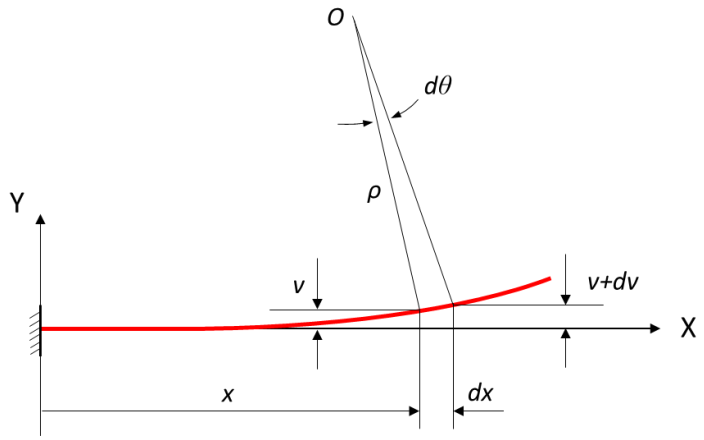

Figure 37. Deflection curve of a beam.

The relationship between the curvature of a beam (k) and its deflection (v) is expressed by the following equation assuming that the angle of rotation or deflection slope is very small ($dv/dx << 1$):

$$k = \frac{1}{\rho} = \frac{d^2v}{dx^2}$$

Deflection $v(x)$ represents the displacement in the direction perpendicular to the axis of the beam of any point on the axis x of the beam, whereas the curvature k is the reciprocal of the radius of curvature ρ of the deformed beam. If the material of the beam is linearly elastic and follows Hooke's law, the curvature can also be written as:

$$k = \frac{1}{\rho} = \frac{M}{EI}$$

Where M is the bending moment; E is the Young's modulus and I is the moment of inertia of the needle. The combination of these two equations provides the basic differential equation of the deflection curve of a beam which relates bending moment and deflection:

$$M = EI\frac{d^2v}{dx^2}$$

The deflection $v(x)$ at any section of the beam at distance x from the base can be obtained by integrating twice this differential equation. Therefore knowing the expression of the bending moment at any point of the needle, it is possible to calculate the equation for the deflection at that point.

The application of the above differential equation for calculation of beam deflection is correct under the following assumptions:

- The material is linearly elastic and follows Hooke's law.
- The slope of the deflection curve is very small ((*dv/dx<<1)*.
- Any shear deformations in the beam section are negligible.

Appendix 2: *Calculation of Young's Modulus from experimental data*

Young's Moduli for both types of needles used in the study were obtained experimentally; using beam theory equation for the tip deflection of a cantilever beam of total length 'L' when subject to a point load 'F' at a distance 'a' from its fixed support:

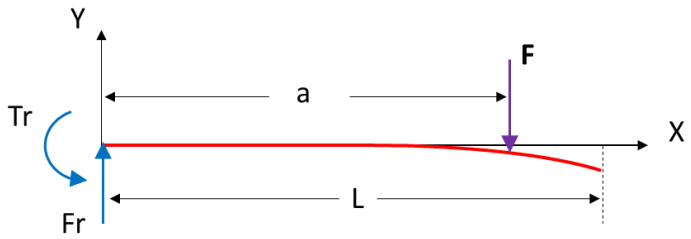

Figure 38. Graphical representation of cantilever beam subject to a point load force F at a certain distance 'a' from its support.

The expression for the tip deflection is: $\delta = \frac{Fa^2}{6EI}(3L - a)$ where E is the Young's Modulus and I is the area Moment of Inertia of the beam.

From the above equation, the value of the Young's Modulus can be calculated when the rest of parameters are known: $E = \frac{Fa^2}{6\delta I}(3L - a)$

For both, Titanium and Plastic needles used in the study, a series of tests were performed where a calibrated weight was suspended from the needle at a known distance from the support base. Tip deflection values were measured at every test from calibrated images and using a ruler scale behind the tip of the needle (Figure 39). Applying the above equation, the Young's Modulus for each needle material can be calculated.

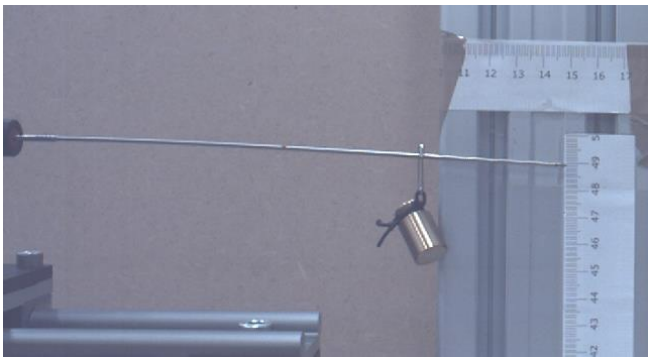

Figure 39. Image for one of the point load deflection experiments. Deflection values were measured through image processing.

The following tables show the parameters used and measured for each test and the resulting value of the Young's Modulus. Needles used for these tests were: Two plastic needles of 200mm length and two Titanium needles 200mm and 250mm long. The average value from all the tests done for the same needle material was the value used as the Young's Modulus of that type of needle for the study.

Plastic Needles – 200 mm Length – 2 mm Diameter				
F (N) - Weight	**a(mm)**	**Deflection (mm)**	**I (mm^4)**	**E (N/mm^2)**
0.1	100	4.01	0.7853982	27094.70685
0.1	150	8.08	0.7853982	27300.58801
0.2	100	7.9	0.7853982	27506.27202
0.2	150	15.55	0.7853982	28371.54355
0.5	100	19.11	0.7853982	28427.46585
0.5	150	36.68	0.7853982	30069.34994
0.1	100	4.19	0.7853982	25930.73377
0.1	150	8.18	0.7853982	26966.83999
0.2	100	8.08	0.7853982	26893.50854
0.2	150	16.24	0.7853982	27166.10236
0.5	100	19.85	0.7853982	27367.70138
0.5	150	38.49	0.7853982	28655.3327
Average Young's Modulus for Plastic Needles				**27645.85**

Titanium Needle – 200mm Length – 1.65 mm Diameter				
F (N) - Weight	**a(mm)**	**Deflection (mm)**	**I (mm^4)**	**E (N/mm^2)**
0.1	100	3.12	0.3285	83258.531
0.1	150	5.62	0.3285	93842.929
0.2	100	5.57	0.3285	93273.471
0.2	150	9.8	0.3285	107632.094
0.5	100	11.95	0.3285	108688.961
0.5	150	22.39	0.3285	117775.181
0.1	100	2.73	0.3285	95152.607
0.1	150	5.38	0.3285	98029.231
0.2	100	5.35	0.3285	97109.015
0.2	150	9.43	0.3285	111855.198
0.5	100	11.64	0.3285	111583.598
0.5	150	22.19	0.3285	118836.697
Titanium Needle – 250mm Length – 1.65 mm Diameter				
F (N) - Weight	**a(mm)**	**Deflection (mm)**	**I (mm^4)**	**E (N/mm^2)**
0.1	100	3.17	0.3285	105952.718
0.1	150	6.16	0.3285	113413.983
0.2	100	6.16	0.3285	109048.739
0.2	150	11.78	0.3285	118612.926
0.5	100	14.38	0.3285	116783.768
0.5	150	28.32	0.3285	123345.716
0.1	100	3.53	0.3285	95147.342
0.1	150	6.57	0.3285	106336.398
0.2	100	6.2	0.3285	108345.199
0.2	150	12.22	0.3285	114342.085
0.5	100	14.57	0.3285	115260.850
0.5	150	28.63	0.3285	122010.153
Average Young's Modulus for Titanium Needles				**107734.89**

Appendix 3: *Formula for beam deflection under a triangular force distribution*

The basic differential equation of the deflection curve of a beam which relates bending moment and deflection can be written as:

$$M = EI\frac{d^2v}{dx^2} = EIv'' \qquad \text{(Eq. 1)}$$

This case is characterized by a triangular force distribution *q(x)* applied to a portion of the beam length equal to (L-a) with maximum intensity value *q1* at the tip of the beam as represented below:

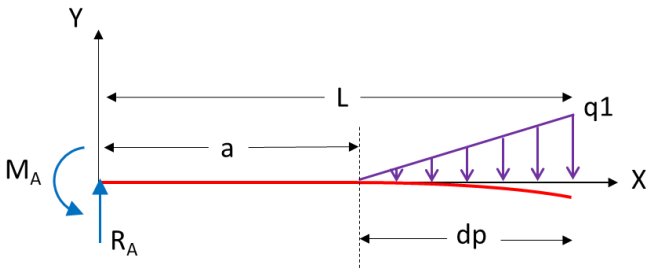

Figure 40. Triangular load distribution acting on the inserted portion of the needle.

1. Reaction force R_A and Moment M_A at the fixed end of the beam are calculated from force and moment equilibrium equations:

$$R_A = \frac{q_1}{2}(L-a)$$

$$M_A = \frac{q_1}{6}.(L-a).(2L+a)$$

2. Due to the discontinuous nature of the loads, there are two different equations for the bending moment of the beam, one for ($x \leq a$) and one for ($a \leq x \leq L$). The bending moment at each region of the beam is obtained from static equilibrium equations at a generic cross-section located a distance x from the base, from the free-body diagrams shown below.

   For $x \leq a$, forces and moments acting on the beam are:

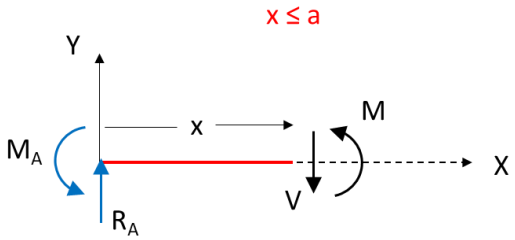

$$\sum \overrightarrow{M}_x = 0 \quad \rightarrow \quad M_A + M - R_A.x = 0$$

Final expression for M after substitution of M_A and R_A:

$$M = \frac{q_1}{6}.(L-a).(3x-2L-a) \qquad (x \leq a) \qquad \text{(Eq.2)}$$

For a ≤ x ≤ L, forces and moments acting on the beam are:

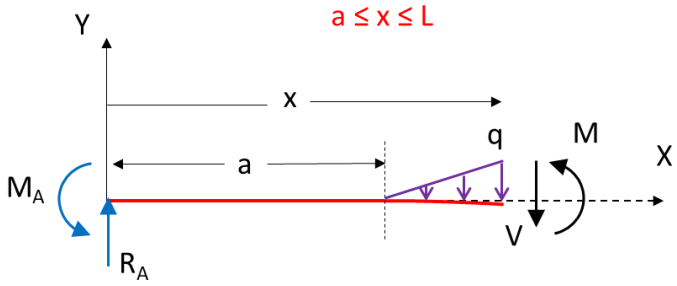

Where: $q = q_1.\frac{(x-a)}{(L-a)}$

$$\sum \overrightarrow{M}_x = 0 \quad \rightarrow \quad M_A + M - R_A.x + \frac{q}{6}.(x-a)^2 = 0$$

Final expression for M after substitution of M_A and R_A and q:

$$M = -\frac{q_1}{6(L-a)}.[(x-a)^3 - 3.x.(L-a)^2 + (L-a)^2.(2L+a)] \qquad (a \le x \le L) \qquad \text{(Eq.3)}$$

3. Differential equations of the deflection curve for the two parts of the beam are obtained by substituting the bending-moment expressions into Eq. 1:

$$EIv'' = \frac{q_1}{6}.(L-a).(3x-2L-a) \qquad (x \le a) \qquad \text{(Eq. 4)}$$

$$EIv'' = -\frac{q_1}{6(L-a)}.[(x-a)^3 - 3.x.(L-a)^2 + (L-a)^2.(2L+a)] \qquad (a \le x \le L)$$

(Eq.5)

4. The first integrations of the two differential equations provide the expressions for the deflection slopes (dδ/dx):

$$v_1'(x) = \frac{q_1}{6EI}.(L-a).\left(\frac{3}{2}x^2 - 2Lx - ax\right) + C_1 \qquad (x \le a) \qquad \text{(Eq. 6)}$$

$$v_2'(x) = -\frac{q_1}{6EI(L-a)}.\left[\frac{(x-a)^4}{4} - \frac{3}{2}(L-a)^2.x^2 + (L-a)^2.(2L+a).x\right] + C_2 \qquad (a \le x \le L)$$

(Eq.7)

The integration constants can be found from the following conditions:

- Deflection slope is zero at *x=0*: $v'(x=0)=0 \rightarrow C_1 = 0$
- Deflection slopes are the same for the two parts of the beam at *x=a*: $v_1'(x=a) == v_2'(x=a)$

Substituting x=a in Eqs. 6 & 7 and making them equal:

$$\frac{-q_1}{12EI}.a.(L-a).(4L-a) = \frac{-q_1}{6EI}.a.(L-a).\left(2L-\frac{a}{2}\right) + C_2 \qquad \rightarrow \qquad C_2 = 0$$

5. The integrations of the slopes give the expressions for the deflections:

$$v_1(x) = \frac{q_1}{6EI}.(L-a).\left(\frac{x^3}{2} - Lx^2 - \frac{a}{2}x^2\right) + C_3 \qquad (x \le a) \qquad \text{(Eq. 8)}$$

$$v_2(x) = -\frac{q_1}{6EI(L-a)}.\left[\frac{(x-a)^5}{20} - \frac{(L-a)^2}{2}x^3 + \frac{(L-a)^2.(2L+a)}{2}.x^2\right] + C_4 \qquad (a \le x \le L) \qquad \text{(Eq.9)}$$

The integration constants can be found from the following conditions:

- Deflection is zero at $x=0$: $v(x=0)=0 \rightarrow C_3 = 0$
- Deflections are the same for the two parts of the beam at $x=a$: $v_1(x=a) = v_2(x=a)$

Substituting $x=a$ in Eqs. 8 & 9 and making them equal:

$$\frac{-q_1}{6EI}.(L-a).a^2.L = \frac{-q_1}{6EI}.(L-a).a^2.L + C_4 \qquad \rightarrow \qquad C_4 = 0$$

6. Therefore the final expressions for the deflection of the beam are:

$$v(x) = \frac{q_1}{6EI}.(L-a).\left(\frac{x^3}{2} - (L+\frac{a}{2}).x^2\right) \qquad (x \le a) \qquad \text{(Eq. 10)}$$

$$v(x) = -\frac{q_1}{120EI(L-a)}.[(x-a)^5 - 10(L-a)^2x^3 + 10(L-a)^2.(2L+a).x^2] \qquad (a \le x \le L) \qquad \text{(Eq. 11)}$$

7. From the last equation the **deflection value at the tip of the beam** ($x = L$) can be extracted:

$$v(x=L) = \delta = -\frac{q_1}{120EI(L-a)}.[(L-a)^5 - 10(L-a)^2L^3 + 10(L-a)^2.(2L+a).L^2] \qquad \text{(Eq. 12)}$$

Replacing $(L-a)$ for d_p, which is the length of the triangular load distribution and the inserted depth in the case of the needle:

$$\boldsymbol{v(x=L) = \delta = \frac{-q_1.d_p}{120EI}(d_p^3 + 10L^3 + 10.a.L^2)} \qquad \textbf{(Eq. 13)}$$

Note: Negative sign of the expression is due to q_1 force being negative in this case and q_1 only accounts for the magnitude value of the force. The sign of the deflection should be the same as the applied q distribution load.

Appendix 4: *Descriptive statistics of influence of different factors on final needle deflection*

Summary statistics of mean and STD values of the three tip deflection variables for all sample groups resulting from possible factor combinations:

Needle	Density	Skin	Speed	dx_end	dy_end	dt_end
Plastic	10%	With skin	Low	1.80 ± 1.00	1.40 ± 1.92	2.78 ± 1.31
			High	1.60 ± 1.22	0.66 ± 1.68	2.49 ± 0.87
		No skin	Low	2.42 ± 0.93	-0.04 ± 1.00	2.58 ± 0.91
			High	2.73 ± 1.20	0.45 ± 1.34	3.08 ± 0.98
	20%	With skin	Low	1.98 ± 1.03	-1.27 ± 0.76	2.50 ± 0.87
			High	2.96 ± 0.62	-0.16 ±1.42	3.18 ± 0.67
		No skin	Low	1.34 ± 1.93	0.52 ± 2.36	2.92 ± 1.08
			High	2.55 ± 1.04	1.30 ± 0.97	3.08 ± 0.61
	5%	No skin	Low	1.44 ± 1.39	-0.89 ± 1.03	2.13 ± 0.95
			High	0.52 ± 0.60	-0.14 ± 0.59	0.81 ± 0.52
Titanium	10%	With skin	Low	1.08 ± 0.51	-0.22 ± 0.91	1.37 ± 0.51
			High	2.03 ± 0.53	0.36 ± 1.17	2.28 ± 0.67
		No skin	Low	-0.12 ± 0.66	-0.91± 0.69	1.15 ± 0.55
			High	0.46 ± 0.92	-0.64 ± 0.58	1.22 ± 0.30
	20%	With skin	Low	-0.32 ± 0.72	-0.13 ± 0.22	0.68 ± 0.37
			High	-0.75 ± 0.53	0.09 ± 0.99	1.16 ± 0.54
		No skin	Low	-0.44 ± 0.67	-0.97 ± 1.14	1.43 ± 0.78
			High	-0.97 ± 0.98	-1.09 ± 0.51	1.71 ± 0.49
	5%	No skin	Low	-0.23 ± 0.88	-0.42 ± 0.61	0.99 ± 0.44
			High	0.11 ± 0.87	-0.18 ± 0.54	0.83 ± 0.49

Table 10. Summary statistics of final needle deflection variables for all possible factor combinations. Maximum and minimum absolute group mean values are marked in red and blue respectively.

Box-plots of tip deflection variables grouped by all existing factor combinations:

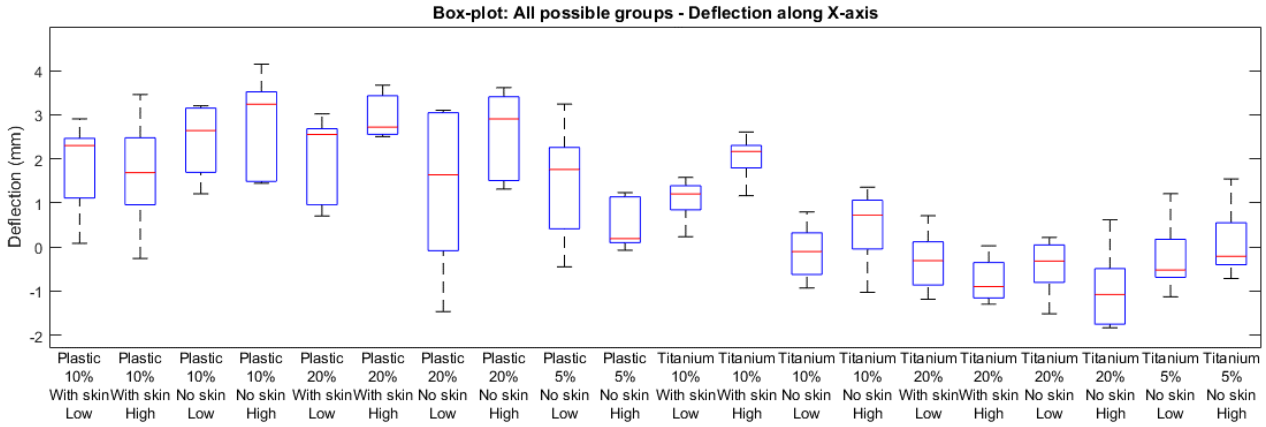

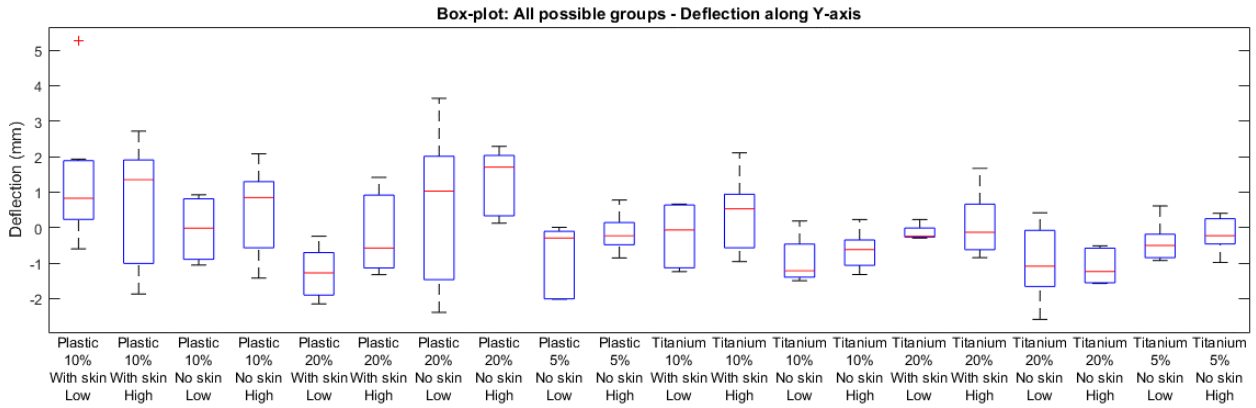

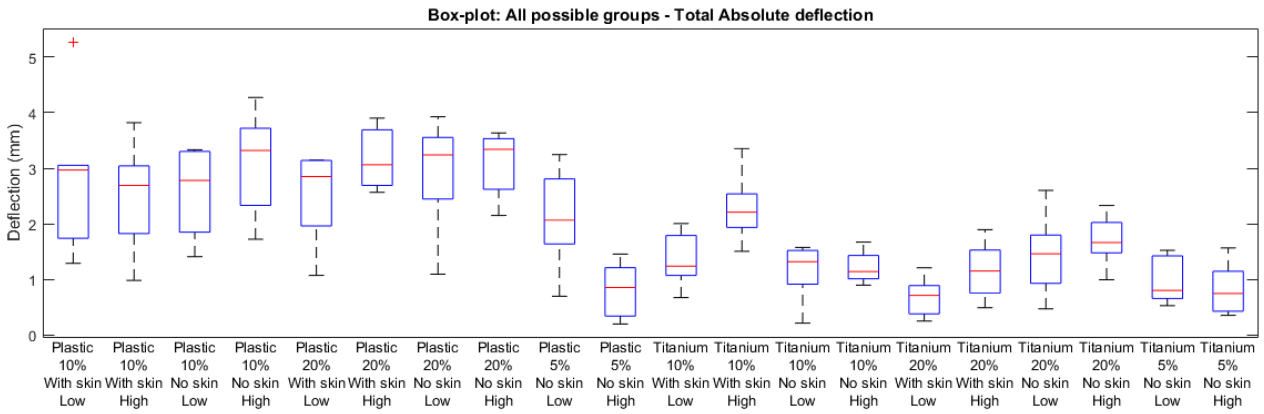

Appendix 5: *Statistical analysis of influence of factors on needle deflection*

Previous tests to check Normality and Homogeneity of Variance of dependent variables (Analysis performed with Matlab):

Variable	**Lilliefors/Kolmogorov-Smirnov Normality Test** (5% significance level)		**Levene's Homogeneity of Variance test** (5% significance level)	
	p-value	**Result**	**p-value**	**Result**
dx_end	0.0591	Accepts normality	0.6644	Accepts homogeneity
dy_end	0.02134	Rejects normality	0.1787	Accepts homogeneity
dt_end	0.004964	Rejects normality	0.8165	Accepts homogeneity

Table 11. Summary of results from Lilliefors/Kolmogorov-Smirnov normality tests and Levene's tests for homogeneity of variance for the three final deflection variables under analysis.

Results from multi-way ANOVAs for the four factors under analysis including two-factor interactions (Analysis performed with R-Commander):

1. Final deflection along X-axis (dx_end):

```
Anova Table (Type II tests)

Response: dx_end
               Sum Sq Df F value    Pr(>F)
density        13.585  2  6.0533 0.0034291 **
needle         74.097  1 66.0331 2.394e-12 ***
skin            1.000  1  0.8909 0.3477757
vel             0.735  1  0.6554 0.4203410
density:needle 19.234  2  8.5706 0.0003945 ***
density:skin    0.011  1  0.0096 0.9221679
needle:skin     6.013  1  5.3586 0.0229211 *
density:vel     1.710  2  0.7619 0.4698003
needle:vel      0.004  1  0.0037 0.9516318
skin:vel        0.344  1  0.3063 0.5813780
Residuals      99.868 89
---
Signif. codes:  0 '***' 0.001 '**' 0.01 '*' 0.05 '.' 0.1 ' ' 1
```

Multiple comparisons for Tissue density factor (Tukey Test):

```
Multiple Comparisons of Means: Tukey Contrasts


Fit: aov(formula = dx_end ~ density, data = Data1)

Linear Hypotheses:
               Estimate Std. Error t value Pr(>|t|)
20% - 10% == 0  -0.8245     0.3124  -2.640   0.0255 *
5% - 10% == 0   -1.0437     0.3810  -2.739   0.0198 *
5% - 20% == 0   -0.2192     0.3917  -0.560   0.8407
---
Signif. codes:  0 '***' 0.001 '**' 0.01 '*' 0.05 '.' 0.1 ' ' 1
(Adjusted p values reported -- single-step method)
```

2. Final deflection along Y-axis (dy_end):

```
Anova Table (Type II tests)

Response: dy_end
               Sum Sq Df F value  Pr(>F)
density         3.667  2  1.2333 0.29625
needle          9.501  1  6.3904 0.01324 *
skin            1.883  1  1.2664 0.26347
vel             2.176  1  1.4635 0.22957
density:needle 10.411  2  3.5013 0.03438 *
density:skin    6.538  1  4.3977 0.03882 *
needle:skin     8.692  1  5.8461 0.01765 *
density:vel     1.190  2  0.4002 0.67139
needle:vel      0.134  1  0.0901 0.76478
skin:vel        0.075  1  0.0501 0.82337
Residuals     132.319 89
---
Signif. codes:  0 '***' 0.001 '**' 0.01 '*' 0.05 '.' 0.1 ' ' 1
```

3. Final absolute total deflection (dt_end):

```
Anova Table (Type II tests)

Response: dt_end
               Sum Sq Df F value    Pr(>F)
density        12.446  2 10.2388 9.951e-05 ***
needle         37.543  1 61.7709 8.431e-12 ***
skin            0.303  1  0.4985   0.48199
vel             0.168  1  0.2766   0.60026
density:needle  4.161  2  3.4230   0.03697 *
density:skin    2.017  1  3.3192   0.07183 .
needle:skin     0.371  1  0.6098   0.43693
density:vel     3.308  2  2.7214   0.07126 .
needle:vel      1.374  1  2.2610   0.13621
skin:vel        0.036  1  0.0600   0.80709
Residuals      54.092 89
---
Signif. codes:  0 '***' 0.001 '**' 0.01 '*' 0.05 '.' 0.1 ' ' 1
```

Multiple comparisons for Tissue density factor (Tukey Test):

```
Multiple Comparisons of Means: Tukey Contrasts


Fit: aov(formula = dt_end ~ density, data = Data1)

Linear Hypotheses:
               Estimate Std. Error t value Pr(>|t|)
20% - 10% == 0  -0.1471     0.2265  -0.649  0.79176
5% - 10% == 0   -0.9834     0.2763  -3.559  0.00162 **
5% - 20% == 0   -0.8363     0.2840  -2.944  0.01106 *
---
Signif. codes:  0 '***' 0.001 '**' 0.01 '*' 0.05 '.' 0.1 ' ' 1
(Adjusted p values reported -- single-step method)
```

Results from non-parametric Kruskal-Wallis tests to reaffirm the influence of the different factors:

	Grouping Factors (p-values)			
Variable	**Needle Type**	**Tissue Density**	**Skin/No skin**	**Insertion speed**
dx_end	9.154e-10 *	0.005976 *	0.0936	0.4701
dy_end	0.02092 *	0.2422	0.09962	0.1276
dt_end	0.00000001237 *	0.001265 *	0.2571	0.518

Table 12. Summary of results from Kruskal-Wallis non-parametric tests to evaluate the effect of the different factors on the three final deflection variables. Statistically significant differences are colour-marked.

Appendix 6: *Statistical comparison of proposed model variants performance*

A *Repeated Measures Analysis of Variance* (ANOVA) with pair-wise comparisons was carried out in order to determine if there were statistically significant differences in the performance of the proposed deflection model variants. For each absolute deflection error variable, the result from each model was considered a repeated measure of the same variable. The whole sample dataset including all the insertion tests was considered for this analysis. A *Tukey-Kramer test* statistic was applied for the multiple comparisons of mean prediction errors between pairs of deflection models. Results from this test are shown in the table below, where a small p-value (<0.05) indicates statistically significant differences between the mean prediction errors of the compared models. All p-values are much lower than 0.05, meaning that all models are significantly different from each other with regard to their mean absolute prediction errors.

Model_1	Model_2	p-values resulting from Multiple Comparisons between Models (*Tukey-Kramer*)			
		Absolute prediction errors at final insertion depth (mm)		Average absolute prediction errors along insertion depth (mm)	
		X-axis	Y-axis	X-axis	Y-axis
1	2	9.59673E-10	9.56049E-10	1.13709E-09	9.56049E-10
1	3	9.56844E-10	9.56049E-10	1.02947E-09	9.56049E-10
2	1	9.59673E-10	9.56049E-10	1.13709E-09	9.56049E-10
2	3	9.12161E-05	9.56049E-10	0.001357992	9.56049E-10
3	1	9.56844E-10	9.56049E-10	1.02947E-09	9.56049E-10
3	2	9.12161E-05	9.56049E-10	0.001357992	9.56049E-10

Table 13. Summary of p-values from pair-wise comparisons (Tukey-Kramer test) between Models regarding their prediction errors (after Repeated Measures ANOVAs). First two columns indicate the models compared.

Appendix 7: *Reliability analysis of final selected model*

Results from two-sample T-tests to verify the equality of means between measured and predicted deflection values along X and Y axes. *p-values* higher than 0.05 indicate that the null hypothesis of equality of means cannot be rejected (h=0) whereas lower *p-values* mean that the test rejects the null hypothesis with a 5% significance level (h=1):

Grouping factors				T-Tests between measured and predicted deflections			
Needle	Tissue Density	Skin	Depth	Deflection in X		Deflection in Y	
				h	p-value	h	p-value
Plastic	10%	No Skin	25mm	1	0.036178064	1	5.53851E-06
Plastic	10%	No Skin	50mm	1	0.007105796	1	2.78786E-05
Plastic	10%	No Skin	75mm	1	0.00061503	1	2.34061E-05
Plastic	10%	No Skin	97mm	1	0.000115756	1	3.31525E-06
Plastic	10%	With Skin	25mm	1	1.479E-05	1	3.45599E-07
Plastic	10%	With Skin	50mm	1	3.70931E-07	1	1.80603E-13
Plastic	10%	With Skin	75mm	1	9.18917E-08	1	2.741E-11
Plastic	10%	With Skin	97mm	1	1.56624E-07	1	3.40131E-10
Plastic	20%	No Skin	25mm	0	0.468288147	1	2.38908E-07
Plastic	20%	No Skin	50mm	0	0.124487364	1	2.20937E-10
Plastic	20%	No Skin	75mm	0	0.071405962	1	2.36366E-08
Plastic	20%	No Skin	97mm	1	0.005445037	1	2.96097E-07
Plastic	20%	With Skin	25mm	1	0.00040932	1	5.12114E-08
Plastic	20%	With Skin	50mm	1	6.49538E-05	1	1.89352E-08
Plastic	20%	With Skin	75mm	1	3.02643E-05	1	2.9925E-07
Plastic	20%	With Skin	97mm	1	1.01267E-05	1	5.20446E-07
Plastic	5%	No Skin	25mm	1	0.002800714	1	0.002538902
Plastic	5%	No Skin	50mm	1	0.001454115	1	0.001576309
Plastic	5%	No Skin	75mm	1	0.041949834	0	0.080931853
Plastic	5%	No Skin	97mm	0	0.60378753	0	0.201988817
Titanium	10%	No Skin	25mm	0	0.80362207	1	0.000420464
Titanium	10%	No Skin	50mm	0	0.319238139	1	0.001808064
Titanium	10%	No Skin	75mm	0	0.669812981	1	0.00104131
Titanium	10%	No Skin	97mm	0	0.631905452	1	0.000150604
Titanium	10%	With Skin	25mm	0	0.156476761	1	0.000432506
Titanium	10%	With Skin	50mm	1	0.002315277	1	7.70539E-09
Titanium	10%	With Skin	75mm	1	0.006153767	1	1.99616E-08
Titanium	10%	With Skin	97mm	1	0.035350542	1	6.40724E-08
Titanium	20%	No Skin	25mm	1	0.03121903	1	9.81965E-08
Titanium	20%	No Skin	50mm	1	0.004560108	1	2.20408E-07
Titanium	20%	No Skin	75mm	1	0.034291341	1	5.5182E-08
Titanium	20%	No Skin	97mm	0	0.45695774	1	5.23922E-07
Titanium	20%	With Skin	25mm	1	0.002662254	1	8.78244E-06
Titanium	20%	With Skin	50mm	1	0.000163557	1	3.68277E-07
Titanium	20%	With Skin	75mm	0	0.151935092	1	3.34181E-11
Titanium	20%	With Skin	97mm	0	0.171223471	1	1.40631E-09
Titanium	5%	No Skin	25mm	1	5.10719E-05	1	0.000121035
Titanium	5%	No Skin	50mm	1	0.000195976	1	0.002364056
Titanium	5%	No Skin	75mm	1	0.003410701	0	0.470768525
Titanium	5%	No Skin	97mm	0	0.109185675	0	0.904523223

Note: Combinations where equality of means cannot be rejected are colour-marked.

Appendix 8: *Detailed comparison of model variants performance*

Summary of mean and STD of the prediction errors of the three model variants considered in the study. These results are for tissue samples without skin layer. Data have been grouped by needle type and tissue density:

Needle	Tissue Density	Model	Group Count	Absolute prediction errors at final insertion depth (mm)		Average absolute prediction errors along insertion depth (mm)	
				X-axis	Y-axis	X-axis	Y-axis
Plastic	5%	1	9	2.23±1.73	0.70±0.42	1.45±0.90	0.57±0.26
		2	9	0.61±0.19	1.79±0.42	0.56±0.22	0.90±0.31
		3	9	0.61±0.31	1.68±0.41	0.54±0.17	0.87±0.30
	10%	1	10	6.14±2.81	3.60±1.76	3.42±1.71	2.18±1.03
		2	10	2.20±1.29	6.06±1.02	1.23±0.72	3.84±0.61
		3	10	2.50±1.39	5.87±1.00	1.35±0.76	3.76±0.60
	20%	1	10	6.21±3.19	7.82±3.44	3.80±1.95	5.62±2.12
		2	10	2.20±1.16	11.80±2.21	1.18±0.65	7.69±1.42
		3	10	2.47±1.35	11.50±2.25	1.28±0.72	7.57±1.44
Titanium	5%	1	10	0.99±0.82	0.35±0.28	0.49±0.28	0.34±0.16
		2	10	0.59±0.30	1.46±0.49	0.67±0.20	0.71±0.26
		3	10	0.50±0.29	1.35±0.44	0.62±0.20	0.67±0.25
	10%	1	10	0.88±0.49	1.14±0.67	0.48±0.25	0.71±0.36
		2	10	0.33±0.21	2.60±0.70	0.29±0.10	1.62±0.41
		3	10	0.33±0.26	2.48±0.68	0.29±0.11	1.58±0.40
	20%	1	10	1.17±0.77	4.07±1.18	0.82±0.46	2.47±0.68
		2	10	0.74±0.63	8.26±2.55	0.68±0.31	5.00±1.47
		3	10	0.70±0.63	7.94±2.43	0.66±0.31	4.87±1.42

Note: The lowest mean prediction errors for each combination are colour-marked.

Appendix 9: *Ethical Review checklist*

University of the West of England
BRISTOL

Faculty of Environment & Technology
Faculty Research Ethics Committee (FET FREC)

ETHICAL REVIEW CHECKLIST FOR UNDERGRADUATE AND POSTGRADUATE MODULES
Please provide project details and complete the checklist below.

Project Details:

Module name	MSc Robotics Dissertation
Module code	UFMED4-60-M
Module leader	Dr Maryam Atoofi
Project Supervisor	Professor Sanja Dogramadzi
Proposed project title	Modelling of brachytherapy needle deflection

Applicant Details:

Name of Student	Carolina Avila Carrasco
Student Number	18044482
Student's email address	Carolina2.Avilacarrasco@live.uwe.ac.uk

	CHECKLIST QUESTIONS	Y/N	Explanation
1.	Does the proposed project involve **human tissue, human participants, environmental damage, the NHS, or data gathered outside the UK**?	N	*If the answer to this is 'N' then no further checks in the list need to be considered.*
2.	Will participants be clearly asked to give consent to take part in the research and informed about how data collected in the research will be used?		
3.	If they choose, can a participant withdraw at any time (prior to a point of "no return" in the use of their data)? Are they told this?		
4.	Are measures in place to provide confidentiality for participants and ensure secure management and disposal of data collected from them?		

CHECKLIST QUESTIONS		Y/N	Explanation
5.	Does the study involve people who are particularly vulnerable or unable to give informed consent (eg, children or people with learning difficulties)?		
6.	Could your research cause stress, physical or psychological harm to anyone, or environmental damage?		
7.	Could any aspects of the research lead to unethical behaviour by participants or researchers (eg, invasion of privacy, deceit, coercion, fraud, abuse)?		
8.	Does the research involve the NHS or collection or storage of human tissue (includes anything containing human cells, such as saliva and urine)?		

Your explanations should indicate briefly for Qs 2-4 how these requirements will be met, and for Qs 5-8 what the pertinent concerns are.

- If Qs 2-4 are answered Yes (Y) and Qs 5-8 are answered No (N), no further reference to the Research Ethics Committee will be required, unless the research plan changes significantly.
- If any of Qs 5-8 are answered Yes (Y), then approval from the Faculty Research Ethics Committee is required *before* the project can start. Approval can take over a month. Please consult with your supervisor about the process.